Contact Mechanics of Inflated Circular Membrane under Large Deformation: Analytical **Solutions**

Xingwei Yang^a, Luxia Yu^a, Rong Long^{a,*}

^a Department of Mechanical Engineering, University of Colorado Boulder, Boulder, CO 80309,

USA.

* Corresponding author: rong.long@colorado.edu

Abstract

Pressurization of thin elastomeric membranes has been exploited as a key actuation mechanism in

soft robotics, leading to soft pneumatic actuators that can deform reversibly upon inflation and

deflation. The contact mechanics of an inflated membrane with another object underlies several

important functionalities of soft pneumatic actuators such as gripping, haptic feedback and

locomotion. Motivated by the technological relevance, we study the contact between an inflated

circular membrane consisting of incompressible neo-Hookean solid and a substrate that is: i) flat

and rigid, ii) spherically curved and rigid, iii) flat and elastic, or iv) spherically curved and elastic.

By assuming that the contact interface is adhesionless and frictionless and that the membrane is

subjected to very large stretch ratios, we obtained approximate analytical solutions for the

membrane's deformation profile as well as the relationship between the applied force,

displacement and contact radius. These solutions agree well with results of numerical simulations.

In particular, when the substrate is elastic, we obtained a dimensionless parameter γ that captures

the transition between two limiting cases, i.e., either the substrate or the inflated membrane is

effectively rigid relative to the other component and thus experiences negligible deformation upon

contact. The analytical solutions provided in this work can offer insights towards designing soft

pneumatic actuators with desired contact compliance.

Keywords

Inflated membrane, large stretch, contact mechanics, Hertzian contact, neo-Hookean model,

analytical solution.

1

1. Introduction

Soft pneumatic actuators, consisting of highly stretchable elastomeric membranes with internal fluidic channels, are capable of reversible large deformation upon inflation and deflation (Rus and Tolley, 2015; Walker et al., 2020). Because of their compliance and deformation capability, soft pneumatic actuators have been widely exploited in soft robotics to enable shape morphing (Rus and Tolley, 2015; Sun et al., 2017), gripping (Guo et al., 2018; Shintake et al., 2018), haptic feedback (Sonar et al., 2020; K. Song et al., 2019) and locomotion (Florez et al., 2014; Shepherd et al., 2011). Many of these functionalities rely on the contact behaviors between soft pneumatic actuators and other objects or surfaces. For example, contact compliance has been recognized as an important property for robotic grippers. The contact between a hard gripper and a soft object (e.g., biomedical implants) may lead to excessive deformation or even damage of the object, while a soft gripper made of inflated elastomeric membrane can provide more conformal contact and less concentrated contact pressure, and thus is more desirable in this scenario (Shintake et al., 2018; Song and Sitti, 2014). Moreover, circular elastomeric membrane, when brought into contact with the human skin upon inflation, can provide haptic feedback that is useful for wearable devices (Sonar et al., 2020; K. Song et al., 2019) and rehabilitation (Shepherd et al., 2011; Yun et al., 2017). Design for these applications requires an in-depth understanding on the contact mechanics of an inflated membrane and another solid, either rigid or elastic. Although simulations based on the Finite Element Method (FEM) have been widely applied to model the contact mechanics of inflated pneumatic actuators (Drotman et al., 2017; Juhari et al., 2005; Li et al., 2014; Zhong et al., 2021), such simulations may be computationally expensive due to the severe nonlinearity associated with large deformation and contact. Analytical solutions, even if approximate, can be useful by allowing quick estimates and efficient exploration of the parametric design space.

Motivated by the discussion above, we study the contact mechanics between an inflated membrane and a substrate. To accommodate various application scenarios, we consider four types of substrates: flat and rigid, spherically curved and rigid, flat and elastic, or spherically curved and elastic. Specifically, we aim to obtain approximate, closed-form analytical solutions revealing deformation profiles of the membrane upon contact, the relationship between the applied force, displacement and contact radius, and how these results depend on system parameters such as the internal pressure. This understanding can lead to guidelines on how to control the contact compliance of inflated membranes. Because the membrane is typically thin and undergoes large

stretch upon inflation, we adopt the nonlinear theory of hyperelastic membrane where bending is neglected (Green and Adkins, 1960; Libai and Simmonds, 1998). The nonlinear membrane theory has been extensively applied in the literature to solve problems involving free inflation of membranes (Hassager et al., 1999; Yang and Feng, 1970; Patil and Dasgupta, 2013) and contact of inflated membranes (Xu and Liechti, 2010; Liu et al., 2018; Liu et al., 2021). To put our work into perspective, we highlight a number of references on the contact mechanics of inflated membranes rather than presenting an exhaustive review. Feng and Yang (1973) studied the frictionless contact of an inflated spherical membrane with two parallel rigid plates, which was revisited by Liu et al. (2018) with more sophisticated friction conditions and experimental characterization. In comparison to the spherical membrane, a more practically relevant loading mode for soft gripper (Carlson et al., 2012; Song and Sitti, 2014) or haptic devices (Sonar et al., 2020) is to pressurize an initially flat circular membrane fixed at its edge. The contact of such inflated circular membrane with a rigid substrate was analyzed by Long et al. (2010) and experimentally studied by Laprade et al. (2013). Patil et al. (2015) analyzed the contact between an inflated circular membrane and a deformable substrate where they simplified the substrate to be an elastic foundation (i.e., a layer of distributed linear springs). The approach of elastic foundation has been applied to the contact problems involving inflated membrane and deformable substrates in various geometries (Patil et al., 2014; Patil and DasGupta, 2015). All of these works accounted for large deformation of the membrane, but had to resort to numerical solutions of the nonlinear governing equations. Existing closed-form analytical solutions for the contact mechanics of inflated circular membranes either required the assumption of small deflection and linear membrane theory (Xu and Liechti, 2010) or relied on simplifications of the deformed geometry (S. Song et al., 2017, 2019; Williams, 1997). Srivastava and Hui (2013) obtained an exact closed-form solution for the frictionless contact between an inflated membrane with large deformation and a rigid substrate, but this solution is for plane strain condition and does not apply to the circular membrane. To the best of our knowledge, thus far there have not been analytical solutions for the axisymmetric contact mechanics of inflated circular membranes, which is the central topic of this work.

The paper is organized as follows. In Section 2, we first describe the geometry, material model and parameters involved in the problem, and follow the approach of Foster (1967a) to obtain general analytical solutions of the membrane under very large stretch. Section 3 presents the

analytical solutions for the inflated membrane in contact with a rigid substrate, which can be either flat or spherically curved. In Section 4, we extend the analytical solutions to consider the contact between an inflated membrane and an elastic substrate, either flat or spherically curved. Comparisons between the approximate analytical solutions and corresponding numerical simulations are also presented. Conclusions are given in Section 5.

2. Analytical Model

2.1 Problem definition

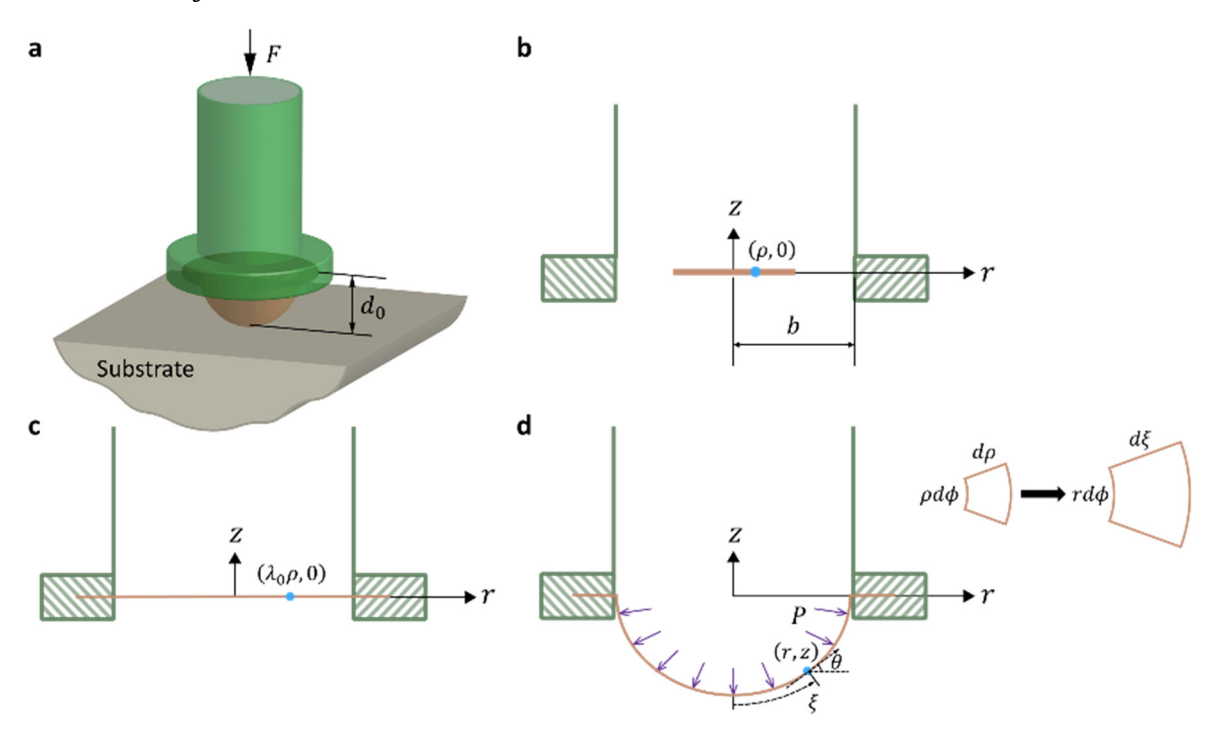


Figure 1 Geometry of the membrane contact problem. (a) Three-dimensional schematic of the pressurized membrane in contact with a substrate. (b-d) The membrane in its (b) undeformed, (c) pre-stretched, and (d) inflated configurations. ξ is the arc length along the cross-sectional curve of the deformed membrane ($\xi = 0$ at r = 0). The inset in (d) shows the top view of a membrane element before and after the deformation.

We consider the contact between a probe of inflated circular membrane and a substrate, as schematically illustrated in Fig.1a. The probe consists of a circular thin membrane with its edge fixed to the end of a pressurization tube. The membrane has a thickness of h in the undeformed configuration (Fig.1b). Axisymmetry allows us to focus on the r-z plane of a cylindrical coordinate system (r, ϕ, z) with the origin located at the center of the circular membrane. The membrane is

first subjected to a uniform biaxial pre-stretch λ_0 and then fixed at its edge at r = b (Fig.1c). The undeformed membrane radius is therefore b/λ_0 . A uniform pressure P is applied on the upper surface of the membrane, and the inflated membrane is brought into contact with the substrate by decreasing the vertical gap, d, between the pressurization tube and the substrate surface. Initially when the inflated membrane and the substrate are in point contact, the gap is equal to the deflection of the membrane's apex under free inflation, denoted as $d_0 (\ge d)$. The contact displacement δ is defined as the difference $d_0 - d$, and the corresponding compressive force is denoted as F. Motivated by the applications in haptic sensing, our goal is to obtain analytical solutions relating F and δ under a prescribed internal pressure P. In case the membrane contact is controlled by varying the internal pressure P (Laprade et al., 2013; S. Song et al., 2017, 2019), one can readily apply the solutions by treating the internal pressure P as the loading parameter.

To facilitate analysis, we make the following assumptions regarding the material and interface models for the membrane and the substrate.

- The contact interface is assumed to be adhesionless and frictionless, i.e., we consider Hertzian contact between the inflated membrane and the substrate.
- The membrane is so thin that its bending rigidity is negligible. Only stretching deformation within the membrane is considered. The membrane material is assumed to follow the incompressible neo-Hookean model with the following strain energy density function:

$$W = \frac{\mu_m}{2} \left(\lambda_1^2 + \lambda_2^2 + \lambda_3^2 - 3 \right) , \tag{1}$$

where μ_m is the shear modulus of the membrane and λ_1 , λ_2 and λ_3 are the principal stretches. Note that incompressibility implies that the out-of-plane stretch λ_3 is related to the two in-plane principal stretches λ_1 and λ_2 by $\lambda_3 = 1/(\lambda_1\lambda_2)$.

Four cases of substrates are considered. In the first two cases (Section 3), the substrate is rigid, but can be flat or spherically curved. In the other two cases (Section 4), the substrate is a linear elastic solid with Young's modulus E_s and Poisson's ratio v_s , and the substrate can still be flat or spherically curved. Although we account for nonlinearity due to large stretch and deflection of the membrane, we still assume linear elasticity for the substrate to apply the Hertz contact theory.

2.2 Large deformation of membrane

Large deformation of hyperelastic membrane has been extensively studied in the literature (Libai and Simmonds, 1998). The equations for kinematics and equilibrium of the hyperelastic membrane adopted in this work closely follow those in Long and Hui (2012). Here we briefly summarize these equations. Deformation of the membrane brings a material point originally located at $(\rho, 0)$ to a new location at (r, z). Let ξ be the longitudinal arc length of the deformed membrane (see Fig.1d). Due to axisymmetry, the two principal stretches, denoted as λ_1 and λ_2 , are given by (see the inset of Fig.1d) (Long and Hui, 2012):

$$\lambda_1 = \frac{d\xi}{d\rho} \,\,\,\,(2)$$

$$\lambda_2 = \frac{r}{\rho} \,. \tag{3}$$

The principal stretch λ_1 is along the arc length ξ direction within the r-z plane (i.e., the longitudinal direction). The other principal stretch λ_2 is along the normal direction of the r-z plane (i.e., the latitudinal direction). The corresponding line tension (force/length) along the longitudinal and latitudinal directions are defined as T_1 and T_2 , respectively. Force balance of an arbitrary area element in the membrane results in the following equilibrium equations (Long and Hui, 2012):

$$T_1 \frac{d\theta}{d\xi} + T_2 \frac{\sin \theta}{r} = P , \qquad (4)$$

$$\frac{d\left(T_{1}r\right)}{dr} = T_{2},\tag{5}$$

where θ is the angle between the longitudinal tangent of the deformed membrane and the r-axis (see Fig.1d) and is determined by the following identity:

$$\cos\theta = \frac{dr}{d\xi}, \ \sin\theta = \frac{dz}{d\xi}.$$
 (6)

Note that eq. (4) is due to equilibrium along the normal direction of the membrane, where $d\theta/d\xi$ and $sin\theta/r$ are the two principal curvatures associated with T_1 and T_2 , respectively. Equation (5) enforces the equilibrium along the longitudinal direction of the membrane. Using the incompressible neo-Hookean model, we obtain the following relationship between the true line tensions (i.e., T_1 , T_2) and the principal stretches (λ_1 , λ_2) (Long and Hui, 2012):

$$T_1 = \mu_m h \left(\frac{\lambda_1}{\lambda_2} - \frac{1}{\lambda_1^3 \lambda_2^3} \right), \ T_2 = \mu_m h \left(\frac{\lambda_2}{\lambda_1} - \frac{1}{\lambda_1^3 \lambda_2^3} \right). \tag{7}$$

We adopt the approximation made by Foster (1967a) that under very large stretch, the term $\lambda_1^{-3}\lambda_2^{-3}$ is negligible in comparison to λ_1/λ_2 or λ_2/λ_1 , i.e.,

$$T_1 \approx \mu_m h \frac{\lambda_1}{\lambda_2} \approx \mu_m^2 h^2 \frac{1}{T_2}. \tag{8}$$

Based on the kinematic, equilibrium and constitutive equations summarized above, one can derive the following result (see Appendix A for details):

$$\sin^2 \theta = \frac{P^2 \left(r^2 + C_1\right)^2}{4\left(\mu_m^2 h^2 r^2 + C_2\right)},\tag{9}$$

where C_2 is an additional integration constant. The constants C_1 and C_2 need to be solved using boundary conditions. Once these two constants are determined, the deformed profile of the membrane, as manifested in the function z(r), can be obtained by integrating $dz/dr = \tan \theta$.

2.3 Free inflation

To demonstrate the utility of eq. (9), we first consider free inflation of the membrane (Fig. 1d). This problem has been solved by Foster (1967b). For completeness, here we rewrite the solution by Foster (1967b) in terms of our notations. The detailed derivation can be found in Appendix B. The deformation profile of the membrane is a spherical cap given by

$$\left(z \pm \sqrt{\left(\frac{2\mu_{m}h}{P}\right)^{2} - b^{2}}\right)^{2} + r^{2} = \left(\frac{2\mu_{m}h}{P}\right)^{2}, \quad 0 \le r \le b \tag{10}$$

The radius of the sphere is

$$R = \frac{2\mu_m h}{P}. (11)$$

The " \pm " sign in eq. (10) implies that there are two possible spherical cap solutions that share the same radius R but are centered at different locations on the z-axis. The deflection at the apex of the membrane due to free inflation, d_0 , is given by

$$d_0 = -z(r=0) = \frac{2\mu_m h}{P} \mp \sqrt{\left(\frac{2\mu_m h}{P}\right)^2 - b^2} . \tag{12}$$

As discussed in Appendix B, the membrane is subjected to equibaxial tension (i.e., $\lambda_1 = \lambda_2$) with $T_1 \approx T_2 \approx \mu_m h$ throughout the entire spherical portion of the inflated membrane. This conclusion will be useful for the contact solutions in Sections 3 and 4.

2.4 Validation using numerical solutions

In a previous work, Long *et al.* (2010) presented numerical solutions for the large deformation of an inflated circular membrane under free inflation or in contact with a flat and rigid substrate. They cast eq. (2)-(6) into a system of ordinary differential equations using the undeformed radial coordinate ρ (see Fig.1b) as the independent variable. We apply the method of Long et al. (2010) to the neo-Hookean membrane and use the resulting numerical solution to validate the analytical solutions. Since the numerical solution is obtained by solving a Boundary Value Problem (BVP), it will be referred to as the BVP solution hereafter.

Figure 2 shows the comparison between the analytical and BVP solutions for free inflation. First, we consider the relation between the pressure P and the deflection d_0 as shown in Fig.2a. The analytical solution in eq. (12) gives a single curve, while the BVP solutions vary with the biaxial pre-stretch λ_0 . When $\lambda_0 = 1$, the analytical solution first deviates from the BVP solution at small deflection d_0 , but converges to it as d_0 increases. This is expected since large d_0 implies large stretch in the membrane, which is the basis for the approximation in eq. (8). The large stretch condition can also be achieved by increasing the pre-stretch λ_0 . As shown in Fig.2a, when $\lambda_0 = 2$, the agreement between the analytical and BVP solutions becomes excellent even for small d_0 . We note that both the analytical and BVP solutions feature a non-monotonic relation between P and d_0 . The existence of a maximum in P implies an instability during pressure-controlled inflation, which is well-known in the literature (Hassager et al., 1999; Osborne and Sutherland, 1909; Patil and Dasgupta, 2013). This pressure maximum, denoted as $P = P_c$ at $d_0 = d_{0c}$, divides the pressure versus deflection curve into a stable ($d_0 < d_{0c}$) and an unstable branch ($d_0 > d_{0c}$), as reflected by the two possible cases in eq. (10). In both cases the membrane deforms to a spherical cap. We will refer to the case with smaller deflection (stable branch) as Case I, and the case with larger

deflection (unstable branch) as Case II, as illustrated in Fig.2b. According to eq. (12), the maximum pressure is

$$P_c = \frac{2\mu_m h}{b}$$
 and $d_{0c} = b$, (13)

indicating that the pressure maximum is achieved when the membrane is inflated into a hemisphere, since b is the radius of the pre-stretched membrane. It should be noted that eq. (13) may slightly overestimate P_c and underestimate d_{0c} for low pre-stretch ($\lambda_0 < \sim 1.5$) due to the approximation in eq. (8).

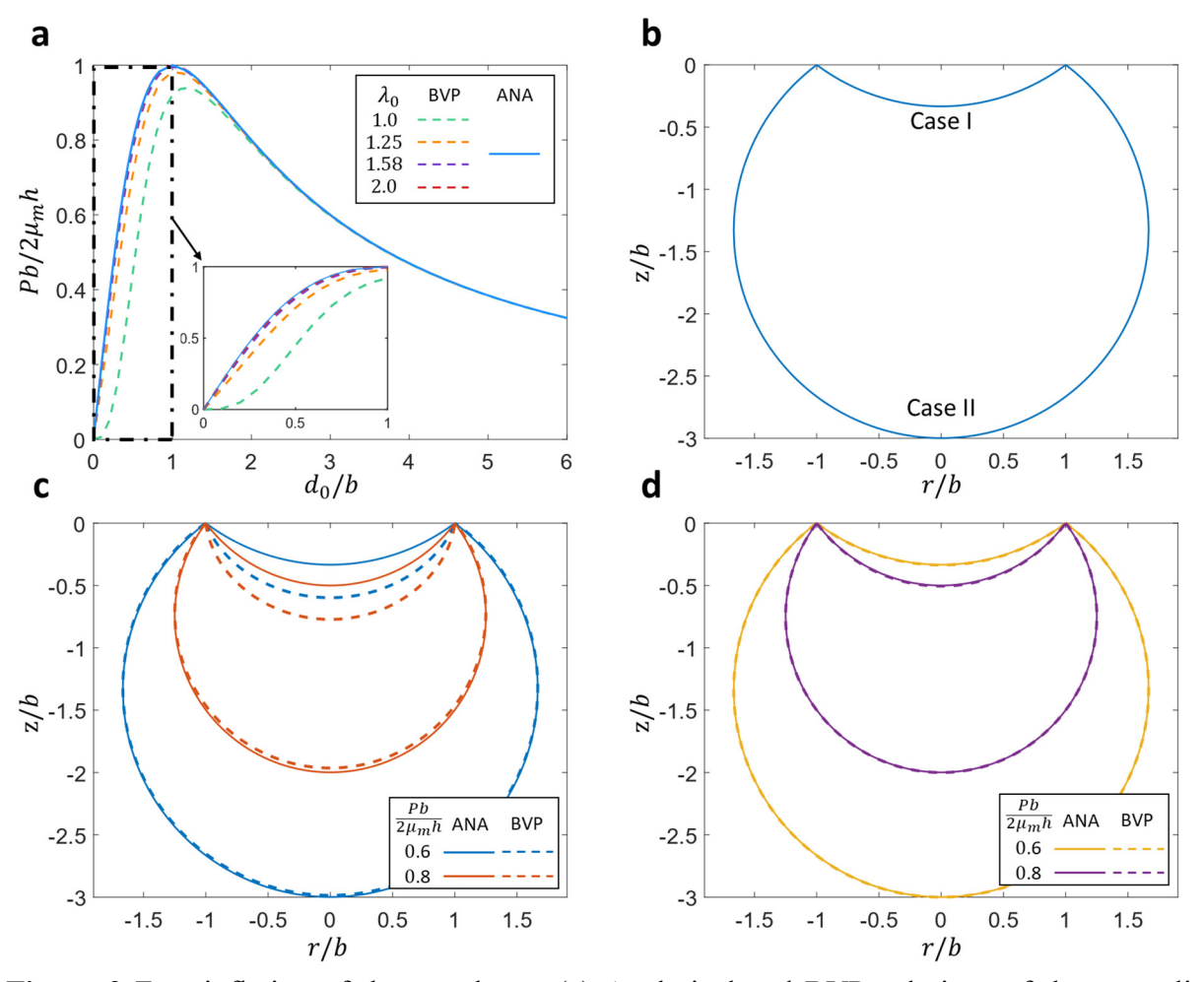


Figure 2 Free inflation of the membrane (a) Analytical and BVP solutions of the normalized pressure versus the normalized deflection for different pre-stretch ratios. (b) Case I and II of membrane deformation profile under $Pb/2\mu_m h = 0.6$ and $\lambda_0 = 1$. (c-d) Analytical and BVP solutions of the membrane deformation profiles for (c) $\lambda_0 = 1$ and (d) $\lambda_0 = 2$.

Figures 2c and 2d compare the membrane deformation profiles without pre-stretch ($\lambda_0 = 1$) or with pre-stretch ($\lambda_0 = 2$), respectively. The curves with the same color represent the two possible cases under the same pressure. The significant difference between analytical and BVP solutions for Case I in Fig.2c confirms the discrepancy observed for $d_0 < d_{0c}$ and $\lambda_0 = 1$. For Case II, the membrane stretch is sufficiently large to ensure accuracy of the analytical solution even without pre-stretch. In Fig.2d, the introduction of pre-stretch substantially improves the accuracy of analytical solutions and we observe excellent agreement between analytical and BVP solutions for both Case I and II.

3. Contact with a rigid substrate

In this section, we consider the contact of an inflated membrane with a rigid substrate which can be flat (Section 3.1) or spherically curved (Section 3.2). Our approach is to divide the membrane into two parts: the contacting part which conforms to the substrate and the free standing part which follows eq. (9). These two parts are jointed at the perimeter of the contact region, where appropriate boundary conditions are prescribed to ensure continuity and equilibrium.

3.1 Contact with a flat rigid substrate

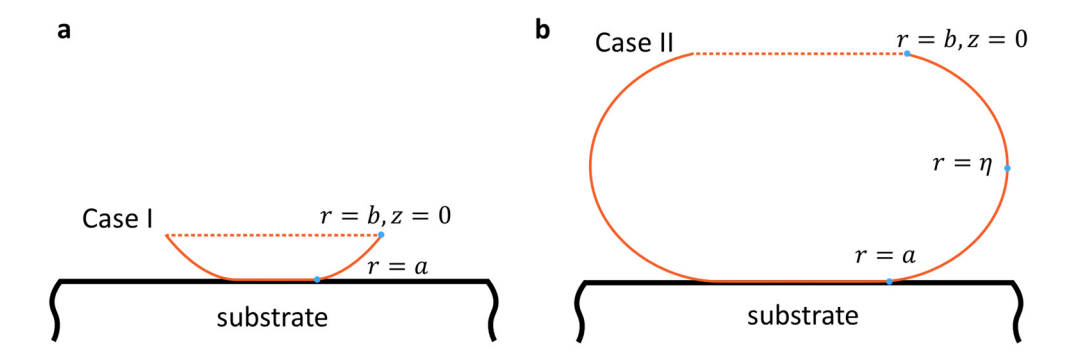


Figure 3 Schematics of the inflated membrane in contact with a flat rigid substrate: (a) Case I and (b) Case II.

As illustrated in Fig.3, the contacting membrane on the flat rigid substrate occupies a circular region of radius a and is under uniform biaxial stretch due to the frictionless condition on the interface (Long et al., 2010). The adhesionless condition implies that both the tangent angle θ and

the stretch ratios (λ_1 and λ_2) should be continuous at the contact edge, otherwise force balance across the contact edge cannot be satisfied (Long et al., 2010). Therefore, we obtain the following boundary conditions for the free standing membrane:

$$\theta = 0$$
 and $\lambda_1 = \lambda_2$ at $r = a$. (14)

These boundary conditions allow us to determine the constants C_1 and C_2 in eq. (9). Specifically, substituting $\theta = 0$ at r = a into eq. (9) yields $C_1 = -a^2$. The biaxial stretch condition $\lambda_1 = \lambda_2$ implies that $T_1 = T_2 \approx \mu_m h$ at r = a, based on which we obtain $C_2 = 0$ by comparing eq. (A2) in Appendix A and eq. (9). Consequently, eq. (9) becomes

$$\sin^2 \theta = \frac{P^2 \left(r^2 - a^2\right)^2}{\left(2\mu_m hr\right)^2} = \left(\frac{r^2 - a^2}{Rr}\right)^2. \tag{15}$$

Recall that R is the radius of the membrane under free inflation in eq. (11). Substituting eq. (15) into eq. (6) gives

$$\frac{dz}{dr} = \tan \theta = \pm \sqrt{\frac{\sin^2 \theta}{1 - \sin^2 \theta}} = \pm \frac{\left(r^2 - a^2\right)}{\sqrt{R^2 r^2 - \left(r^2 - a^2\right)^2}}.$$
 (16)

Integrating eq. (16) yields

$$z = \pm \int \frac{\left(r^2 - a^2\right)}{\sqrt{R^2 r^2 - \left(r^2 - a^2\right)^2}} dr + C_4,$$
 (17)

where C_4 is a constant to be determined by boundary conditions. To simplify notation, we normalize all lengths by the radius of the pre-stretched membrane before inflation, b, and define a new integral function:

$$\Psi(r; \overline{a}, \overline{R}) = \frac{1}{b} \int_{a}^{r} \frac{\left(s^{2} - a^{2}\right)}{\sqrt{R^{2}s^{2} - \left(s^{2} - a^{2}\right)^{2}}} ds = \int_{\overline{a}}^{r/b} \frac{\left(\overline{s}^{2} - \overline{a}^{2}\right)}{\sqrt{\overline{R}^{2}\overline{s}^{2} - \left(\overline{s}^{2} - \overline{a}^{2}\right)^{2}}} d\overline{s},$$
 (18)

where $\overline{s} = s/b$, $\overline{a} = a/b$ and $\overline{R} = R/b$. This function is in closed-form and can be related to elliptic integrals (see Appendix C). The "±" sign in eq. (16) and (17) implies there are two possible contact solutions, which correspond to the two cases for free inflation as elaborated below.

Case I: the membrane deforms into a small spherical cap (i.e., maximum deflection $d_0 < b$) before contacting the substrate. In the free standing membrane, z increases monotonically with r from the contact edge (r = a) to the fixed end (r = b) (see Fig.3a). As a result, we set $0 \le \theta < \pi/2$ and take the "+" sign in eq. (17) and obtain the following solution by enforcing z = 0 at r = b:

$$z/b = \Psi(r; \overline{a}, \overline{R}) - \Psi(b; \overline{a}, \overline{R}), \qquad a \le r \le b.$$
 (19)

The contact displacement δ can be calculated by subtracting the vertical gap, i.e., d = -z (r = a), from the initial value d_0 in eq. (12), which gives

$$\delta = d_0 - d = R - \sqrt{R^2 - b^2} - b\Psi(b; \overline{a}, \overline{R}). \tag{20}$$

It is worth pointing out that the Case I solution is in agreement with the linear analysis by Xu and Lietchi (2011) provided that the membrane is under sufficiently large pre-stretch and is limited to small deflection. Details of the comparison are given in Appendix D.

Case II: the membrane deforms into a large spherical cap (i.e., maximum deflection $d_{\theta} > b$) before contacting the substrate. The free standing membrane consists of two segments: r first increases ($0 \le \theta < \pi/2$) and then decreases ($\pi/2 \le \theta < \pi$) as z increases (see Fig.3b). The critical point at which r starts to decrease, denoted as $r = \eta$, is determined by seeking where $\theta = \pi/2$. Based on eq. (16), the following equation needs to be satisfied for $\theta = \pi/2$ at $r = \eta$:

$$R^2 \eta^2 - \left(\eta^2 - a^2\right)^2 = 0. {(21)}$$

There are two positive roots of eq. (21): one larger than and the other smaller than the contact radius a, i.e.,

$$\eta = \frac{R + \sqrt{R^2 + 4a^2}}{2} > a, \tag{22}$$

$$\eta' = \frac{-R + \sqrt{R^2 + 4a^2}}{2} < a. \tag{23}$$

For the flat rigid substrate considered here, we exclude η' because geometry of the deformed membrane (see Fig.3b) prevents the possibility that $\theta = \pi/2$ at r < a. Therefore, the two segments of the free standing membrane are jointed at $r = \eta$ as shown in Fig.3b. The upper segment features

dz/dr < 0 and thus we adopt the negative sign in eq. (16). Using the boundary condition that z = 0 at r = b, we obtain the following equation for the upper segment:

$$z/b = \Psi(b; \overline{a}, \overline{R}) - \Psi(r; \overline{a}, \overline{R}), \qquad b \le r \le \eta \text{ and } z \ge z(r = \eta).$$
 (24)

On the lower segment, $dz/dr \ge 0$ and we adopt the positive sign in eq. (16). By enforcing the continuity condition at $r = \eta$, we find the following profile for the lower segment:

$$z/b = \Psi(b; \overline{a}, \overline{R}) + \Psi(r; \overline{a}, \overline{R}) - 2\Psi(\eta; \overline{a}, \overline{R}), \quad a \le r < \eta \text{ and } z < z(r = \eta). \tag{25}$$

Similar to Case I, the contact displacement δ is calculated using d_0 in eq. (12) and d = -z(r = a):

$$\delta = d_0 - d = R + \sqrt{R^2 - b^2} - 2b\Psi(\eta; \overline{a}, \overline{R}) + b\Psi(b; \overline{a}, \overline{R}). \tag{26}$$

For both Case I and II, we determine the compressive contact force F by integrating the contact pressure between the membrane and the substrate. Since the contacting membrane is flat, the contact pressure P^* must be uniform and equal to the internal pressure P. Therefore, F is given by

$$F = \pi a^2 P. (27)$$

To summarize, eq. (19) and eq. (24)-(25), when jointed by the flat contacting membrane ($0 \le r < a$), provide the deformation profile of the membrane in Case I and II, respectively. The relation between the compressive contact force F and the contact displacement δ can be determined by combining eq. (20) and (27) for Case I and eq. (26) and (27) for Case II. These analytical solutions do not explicitly depend on the pre-stretch λ_0 , but depend on two parameters: $\overline{a} \equiv a/b$ and $\overline{R} \equiv R/b$. The former measures the size of the contact region, while the latter reflects the internal pressure P through $R = 2\mu_m h/P$.

3.2 Contact with a spherically curved rigid substrate

Here we consider the scenario where the rigid substrate is spherically curved with a radius R_s . We assume the center of the substrate is located on the z-axis (i.e., vertically aligned with the center of the membrane) to maintain axisymmetric contact. The contacting membrane conforms to the curved substrate and has a spherical profile. Because of the frictionless condition, the contacting membrane is only subjected to the internal pressure P and the normal contact pressure P_e from the

interface. Effectively, the contacting membrane is inflated by the pressure differential $P_e - P$. Based on the results in Section 2.3, we conclude that $P_e - P$ is uniform due to the spherical profile of the contacting membrane. The radius of the contacting membrane is the same as that of the substrate, R_s . According to eq. (11), we have

$$P_e - P = \frac{2\mu_m h}{R_s},\tag{28}$$

where we have adopted the sign convention that $R_s < 0$ ($P_e < P$) if the substrate is concave and $R_s > 0$ ($P_e > P$) if the substrate is convex (see Fig.4).

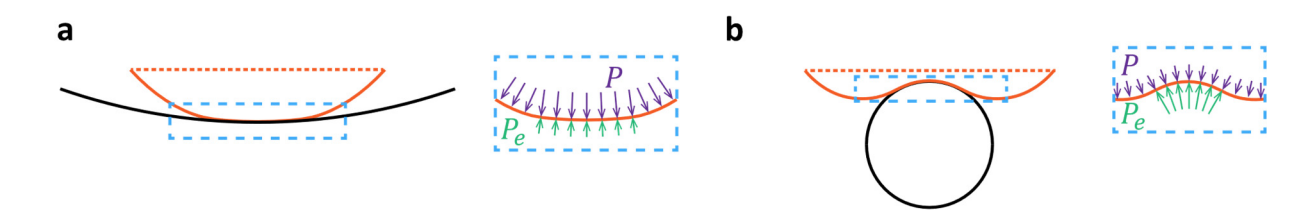


Figure 4 Schematics of the inflated membrane in contact with a spherically curved rigid substrate. (a) Concave substrate: $P > P_e$. (b) Convex substrate: $P < P_e$. For simplicity, only Case I membrane deformation is shown.

For the free standing membrane, we first determine the boundary conditions at the contact edge. Similar to the flat rigid substrate, the adhesionless contact condition implies that the tangent angle θ and the stretch ratios (λ_1 and λ_2) are continuous at the contact edge. Since the contacting membrane is subjected to equibiaxial stretch due to its spherical profile, we enforce $\lambda_1 = \lambda_2$ at r = a. The tangent angle θ at the contact edge is no longer 0, but is equal to θ_0 such that

$$\sin \theta_0 = -\frac{a}{R_s} \,. \tag{29}$$

Note that $\theta_0 > 0$ for concave substrate and $\theta_0 < 0$ for convex substrate. Plugging the boundary conditions, i.e., $\theta = \theta_0$ and $\lambda_1 = \lambda_2$ at r = a, into eq. (9) and eq. (A2) in Appendix A, we have

$$C_1 = \frac{2\mu_m ha \sin \theta_0}{P} - a^2, C_2 = 0.$$
 (30)

Note that $C_2 = 0$ is due to the equibiaxial stretch condition at the contact edge. Combining eq. (9), (11), (29) and (30), we arrive at the following equation for the free standing membrane:

$$\sin^2 \theta = \frac{\left(r^2 - \left(1 + \frac{R}{R_s}\right)a^2\right)^2}{R^2 r^2} \,. \tag{31}$$

To simplify notation, we define

$$\zeta = \frac{R\sin\theta_0}{a} = -\frac{R}{R_0}. (32)$$

Similar to Section 3.1, we first use eq. (31) to calculate dz/dr, i.e.,

$$\frac{dz}{dr} = \tan \theta = \pm \frac{\left(r^2 - (1 - \zeta)a^2\right)}{\sqrt{R^2 r^2 - \left(r^2 - (1 - \zeta)a^2\right)^2}}.$$
 (33)

Integrating eq. (33) yields

$$z = \pm \int \frac{\left(r^2 - (1 - \zeta)a^2\right)}{\sqrt{R^2 r^2 - \left(r^2 - (1 - \zeta)a^2\right)^2}} dr + C_5, \tag{34}$$

where the " \pm " indicates that the free standing membrane may contain segments with dz/dr > 0 or dz/dr < 0. The integration constant C_5 can be determined using the boundary condition z = 0 at r = b, which depends on the detailed contact conditions as discussed in the following three subsections. To facilitate discussion, we introduce a new integral function:

$$\Phi(r; \overline{a}, \overline{R}, \zeta) = \frac{1}{b} \int_{a}^{r} \frac{\left(s^{2} - (1 - \zeta)a^{2}\right)}{\sqrt{R^{2}s^{2} - \left(s^{2} - (1 - \zeta)a^{2}\right)^{2}}} ds = \int_{\overline{a}}^{x/b} \frac{\left(\overline{s}^{2} - (1 - \zeta)\overline{a}^{2}\right)}{\sqrt{\overline{R}^{2}\overline{s}^{2} - \left(\overline{s}^{2} - (1 - \zeta)\overline{a}^{2}\right)^{2}}} d\overline{s} , \quad (35)$$

where $\overline{s} \equiv s/b$, $\overline{a} \equiv a/b$ and $\overline{R} \equiv R/b$. This function is similar to that in eq. (18) but is enriched by the additional parameter $\zeta = -R/R_s$ due to the spherically curved substrate.

3.2.1 Concave substrate

For concave substrate, R_s is negative and we assume $|R_s|$ is larger than the radius of the freely inflated membrane R, otherwise an annular contact region would be established before the apex of the membrane reaches the substrate. Effectively we limit our solution to the regime 0 < 1

 ζ < 1. Following the same procedures in Section 3.1, we obtain solutions for Case I and Case II using the ranges of r illustrated in Fig.5.

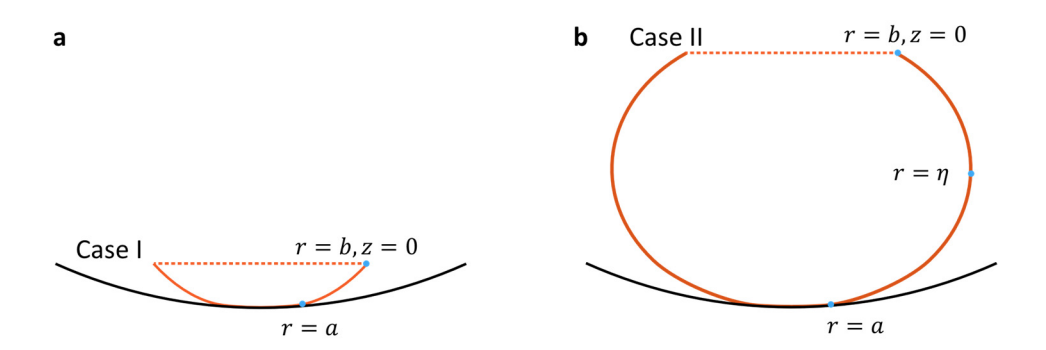


Figure 5 Schematics of the inflated membrane in contact with a concave rigid substrate: (a) Case I and (b) Case II.

Case I: we require $0 \le \theta_0 \le \theta < \pi/2$ and dz/dr > 0 throughout the free standing membrane (see Fig.5a) and enforce the boundary condition z = 0 at r = b, which yields

$$z/b = \Phi(r; \overline{a}, \overline{R}, \zeta) - \Phi(b; \overline{a}, \overline{R}, \zeta), \qquad a \le r \le b.$$
 (36)

Unlike the flat rigid substrate, the contacting membrane also contributes to the vertical gap $d \equiv -z(r=0)$: d is equal to the deflection of the free standing membrane plus the height of the contacting membrane:

$$d = -z(r = a) - R_s - \sqrt{R_s^2 - a^2} . {37}$$

Recall that $R_s < 0$. The contact displacement δ is given by

$$\delta = d_0 - d = R - \sqrt{R^2 - b^2} - b\Phi(b; \overline{a}, \overline{R}, \zeta) + R_s + \sqrt{R_s^2 - a^2}.$$
 (38)

Case II: similar to Section 3.1, we first determine the critical points at which the tangent angle $\theta = \pi/2$ by setting the denominator within the integral of eq. (34) to zero and solve for r. There are two positive solutions $r = \eta$ and η' :

$$\eta = \frac{R + \sqrt{R^2 + 4(1 - \zeta)a^2}}{2},$$
(39)

$$\eta' = \frac{-R + \sqrt{R^2 + 4(1 - \zeta)a^2}}{2}.$$
 (40)

Since $0 < \zeta < 1$, it is clear that $\eta' < a$ and thus we exclude this solution. On the other hand, geometrical consideration dictates that the contact radius a cannot exceed the substrate radius, i.e., $a \le |R_s|$. Using this constraint, one can show that $\eta \ge a$. Therefore, we divide the free standing membrane into two segments at $r = \eta$. Deformation profiles for these two segments are given by

Upper:
$$z/b = \Phi(b; \overline{a}, \overline{R}, \zeta) - \Phi(r; \overline{a}, \overline{R}, \zeta), \quad b \le r \le \eta \text{ and } z \ge z(r = \eta),$$
 (41)

Lower:
$$z/b = \Phi(b; \overline{a}, \overline{R}, \zeta) + \Phi(r; \overline{a}, \overline{R}, \zeta) - 2\Phi(\eta; \overline{a}, \overline{R}, \zeta), a \le r < \eta \text{ and } z < z(r = \eta).$$
 (42)

To determine the contact displacement δ , we substitute z(r=a) from eq. (42) into eq. (37) to calculate the vertical gap d and obtain

$$\delta = d_0 - d = R + \sqrt{R^2 - b^2} - 2\Phi\left(\eta; \overline{a}, \overline{R}, \zeta\right) + \Phi\left(b; \overline{a}, \overline{R}, \zeta\right) + R_s + \sqrt{R_s^2 - a^2} . \tag{43}$$

For both Case I and Case II, the compressive contact force F can be calculated by integrating the contact pressure P_e projected along the z-direction, i.e.,

$$F = \pi a^2 P_e = \pi a^2 P(1 - \zeta), \tag{44}$$

where we have used eq. (28) to determine P_e and eq. (11) and (32) to simplify the expression.

3.2.2 Convex substrate: contact with upper hemisphere

For convex substrate, R_s is positive and hence $\zeta = -R/R_s < 0$. Solution of the membrane deformation depends on whether the contact region remains on the upper hemisphere of the substrate or extends to the lower hemisphere. We first consider membrane contact with the upper hemisphere of the substrate. As illustrated in Fig.6, the contact radius a must be smaller than R_s . Within the contact region, the membrane has the same convex curvature as the substrate. As a result, the tangent angle at the contact edge, θ_0 , falls into the range of $-\pi/2 \le \theta_0 \le 0$ as given by eq. (29). The negative θ_0 implies that in the free standing membrane z must decrease first as one moves away from the contact edge (r = a). As r is increased, the free standing membrane may reach a

point where the tangent angle $\theta = 0$. We denote this point as $r = \chi$ and calculate it by setting $\tan \theta = 0$ in eq. (33), which yields

$$\chi = a\sqrt{1-\zeta} \ . \tag{45}$$

It is clear that $\chi > a$ because $\zeta < 0$. Next, we discuss solutions for Case I and Case II shown in Fig.6.

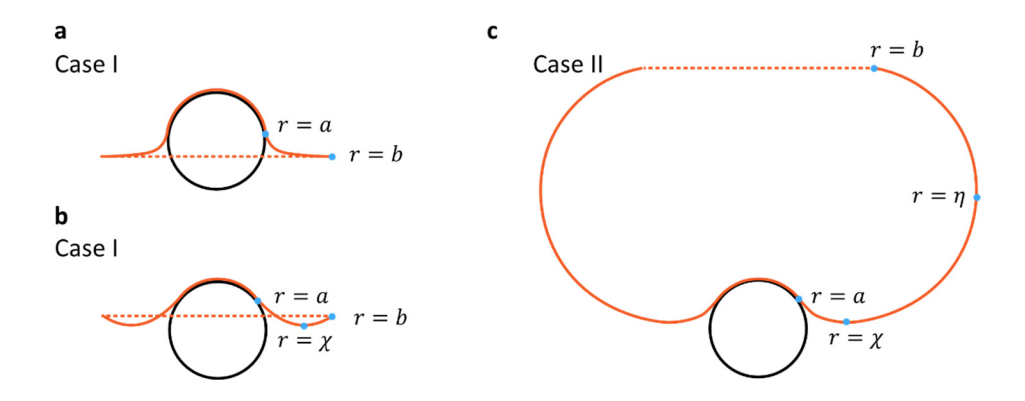


Figure 6 Schematics of the inflated membrane in contact with the upper hemisphere of the convex substrate. (a) Case I with $\chi \ge b$. (b) Case I with $\chi \le b$. (c) Case II.

Case I: two possibilities exist depending on whether χ is larger or smaller than b. If $\chi \ge b$, z would decrease monotonically with r for $a \le r \le b$, i.e., $-\pi/2 \le \theta_0 \le \theta \le 0$ throughout the free standing membrane (see Fig.6a). If $\chi < b$, z would first decrease with increasing r in the interval $a \le r \le \chi$ and then increase with increasing r in the interval $\chi < r \le b$ (see Fig.6b). The range of tangent angle θ in the free standing membrane is expanded to $-\pi/2 \le \theta_0 \le \theta < \pi/2$. Interestingly, both possibilities can be accounted for by taking the "+" sign in eq. (33). Specifically, the possible change in sign of dz/dr (or $\tan \theta$) at $r = \chi$ is accommodated by the numerator $(r^2 - (1 - \zeta)a^2)$ which changes from negative to positive as r increases beyond χ . Therefore, whether $\chi \ge b$ or $\chi < b$, deformation profile of the free standing membrane is still given by eq. (36). Because the point at $r = \chi$ does not involve a change of sign in eq. (33), we will not divide the free standing membrane at this point in the subsequent discussions. The vertical gap d, defined as -z(r = 0), is now equal

to the deflection of the free standing membrane subtracted by the height of the contacting membrane due to the convex curvature of the substrate:

$$d = -z(r = a) - (R_s - \sqrt{R_s^2 - a^2}). (46)$$

Accordingly, the contact displacement δ is given by

$$\delta = d_0 - d = R - \sqrt{R^2 - b^2} - b\Phi(b; \overline{a}, \overline{R}, \zeta) + R_s - \sqrt{R_s^2 - a^2}.$$
 (47)

Case II: by comparing eq. (39) and (45), we conclude that $\eta > \chi$ (see Fig.6c). As discussed above, we can treat the free standing membrane within $a \le r \le \eta$ as a single segment by taking the "+" sign in eq. (33). The other segment with $b \le r < \eta$ can be accounted for by taking the "-" sign in eq. (33). Therefore, deformation profile of the free standing membrane is still given by eq. (41) and (42). Similar to Case I, we use eq. (46) to calculate the vertical gap d. The corresponding contact displacement δ is

$$\delta = d_0 - d = R + \sqrt{R^2 - b^2} - 2b\Phi(\eta; \overline{a}, \overline{R}, \zeta) + b\Phi(b; \overline{a}, \overline{R}, \zeta) + R_s - \sqrt{R_s^2 - a^2}. \tag{48}$$

For both Case I and Case II, the contact force F can still be calculated using eq. (44).

3.2.3 Convex substrate: contact with lower hemisphere

When the contacting membrane extends to the lower hemisphere of the substrate (see Fig.7), the tangent angle at the contact edge, θ , falls into the range of $-\pi \le \theta$, $<-\pi/2$ as given by eq. (29). The main difference between this scenario and that considered in Section 3.2.2 is that r first decreases immediately outside the contact region. Consequently, both solutions for the critical points, i.e., η and η' in eq. (39) and (40), are permitted. Since $\zeta < 0$ and $a \le R_s$, one can show that $\eta > a$ and $\eta' < a$. The point at $r = \eta$ features $\theta = \pi/2$, while the point at $r = \eta'$ features $\theta = -\pi/2$. The existence of $r = \eta'$ introduces a new segment to the free standing membrane as compared to the upper hemisphere contact considered in Section 3.2.2 (Fig.7). Following procedures similar to those in Section 3.2.2, we find the solutions for two cases of lower hemisphere contact as summarized below.

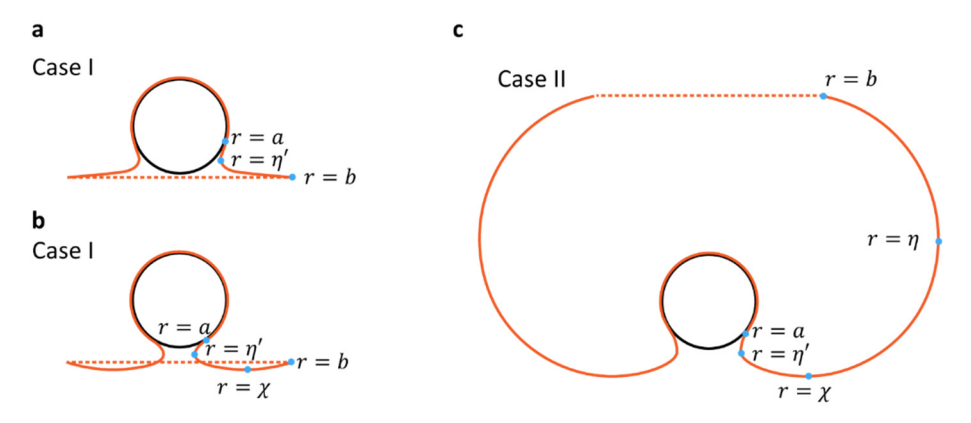


Figure 7 Schematics of the inflated membrane in contact with the lower hemisphere of the convex substrate. (a) Case I with $\chi \ge b$. (b) Case I with $\chi \le b$. (c) Case II.

Case I: the free standing membrane starts at the contact edge (r = a) with $-\pi \le \theta_0 \le \theta < -\pi/2$ for r in the interval $\eta' < r \le a$, where we adopt "—" sign in eq. (33). After that, whether $\chi \ge b$ or $\chi < b$ (see Fig.7a and 7b), we can treat the free standing membrane as one segment with $\eta' \le r \le b$ and $-\pi/2 \le \theta < \pi/2$, where we adopt the "+" sign in eq. (33). Enforcing the boundary condition and continuity condition, we obtain the following solutions for the deformation profile of the free standing membrane:

$$z/b = \Phi(r; \overline{a}, \overline{R}, \zeta) - \Phi(b; \overline{a}, \overline{R}, \zeta), \qquad \eta' \le r \le b, \qquad (49)$$

and

$$z/b = 2\Phi(\eta'; \overline{a}, \overline{R}, \zeta) - \Phi(r; \overline{a}, \overline{R}, \zeta) - \Phi(b; \overline{a}, \overline{R}, \zeta), \qquad \eta' < r \le a.$$
 (50)

The vertical gap $d \equiv -z(r = 0)$ is given by

$$d = -z(r = a) - (R_s + \sqrt{R_s^2 - a^2}).$$
(51)

Note that the height of the contacting membrane is different from that in eq. (46) because of the contact region extends to the lower hemisphere of the substrate. The contact displacement δ is

$$\delta = d_0 - d = R - \sqrt{R^2 - b^2} + 2b\Phi(\eta'; \overline{a}, \overline{R}, \zeta) - b\Phi(b; \overline{a}, \overline{R}, \zeta) + R_s + \sqrt{R_s^2 - a^2}.$$
 (52)

Case II: the free standing membrane consists of three segments: i) $-\pi \le \theta_0 \le \theta < -\pi/2$ in $\eta' < r \le a$, ii) $-\pi/2 \le \theta \le \pi/2$ for $\eta' \le r \le \eta$, and iii) $\pi/2 < \theta \le \pi$ for $b \le r < \eta$. Among these three

segments, i) and iii) require the "-" sign in eq. (33), while ii) requires the "+" sign in eq. (33). Again, by enforcing boundary condition and continuity conditions, we obtain the following solutions for the deformation profile of the free standing membrane

$$z/b = \Phi(b; \overline{a}, \overline{R}, \zeta) - \Phi(r; \overline{a}, \overline{R}, \zeta), \qquad b \le r < \eta, \qquad (53)$$

$$z/b = \Phi(b; \overline{a}, \overline{R}, \zeta) + \Phi(r; \overline{a}, \overline{R}, \zeta) - 2\Phi(\eta; \overline{a}, \overline{R}, \zeta), \quad \eta' \le r \le \eta, \quad (54)$$

and

$$z/b = -\Phi(r; \overline{a}, \overline{R}, \zeta) + 2\Phi(\eta'; \overline{a}, \overline{R}, \zeta) - 2\Phi(\eta; \overline{a}, \overline{R}, \zeta) + \Phi(b; \overline{a}, \overline{R}, \zeta), \quad \eta' < r \le a. \quad (55)$$

Using eq. (51), we can calculate the vertical gap d and the resulting contact displacement δ is

$$\delta = R + \sqrt{R^2 - b^2} - 2b\Phi(\eta; \overline{a}, \overline{R}, \zeta) + 2b\Phi(\eta'; \overline{a}, \overline{R}, \zeta) + b\Phi(b; \overline{a}, \overline{R}, \zeta) + R_s + \sqrt{R_s^2 - a^2}.$$
 (56)

Similar to Section 3.2.2, the contact force F for both Case I and Case II can be calculated using eq. (44).

3.3 Validation using BVP and FEM results

In this section, we verify the accuracy of our analytical solutions for membrane contact using numerical results. Since our analytical solutions are based on the large-stretch approximation in eq. (8), their accuracy is improved under a larger pre-stretch λ_0 . Therefore, for verification purpose, we set $\lambda_0 = 2$ for all results in this section. According to Section 2.4, this pre-stretch is sufficient for the analytical solution to accurately capture free inflation of the membrane. We first apply the numerical method in Long et al. (2010), which will be referred to as the BVP solution and is limited to the contact with flat rigid substrate. To enable comparison for membrane contact with spherically curved substrate, we build a FEM model using the commercial software ABAQUS (version 2020, Simulia, Providence, RI, USA). Details of the FEM model are provided in Appendix E. Since the Case II solution resides on the unstable branch of the *P* versus d_0 curve in Fig2a, our FEM model in ABAQUS was unable to access the Case II solution due to the controlled internal pressure *P*. Therefore, only Case I results were obtained from FEM.

We first validate the solutions for the contact with flat rigid substrate. Figures 8a and 8b show the analytical solutions for the membrane deformation profiles in Case I and Case II with corresponding BVP solutions. Agreement between the two sets of results is evident. In addition, we plot the contact force F as a function of the contact displacement δ for Case I and Case II in Fig.8c and 8d, respectively, showing good agreement between the analytical, BVP and FEM results (Case I only). Interestingly, our analytical solutions reveal that the average contact stiffness, i.e., F/δ , decreases with the internal pressure P in Case I (Fig.8c), but increases with the internal pressure P in Case II (Fig.8d). This reverse of trend from Case I to Case II agrees well with the numerical solutions.

Next, we validate the solutions for the contact with spherically curved rigid substrate. Figures 9a-9c show the excellent agreement between analytical and FEM results for the Case I membrane profiles with concave, convex (upper hemisphere), and convex (lower hemisphere) substrates, respectively. Even with very large contact area (e.g., Fig. 9c), our analytical solutions can still accurately capture the nonlinear deformation of the membrane. Figures 9d-9f show only the analytical solutions for the Case II membrane profiles due to the lack of FEM results. Analytical solutions for the contact force-displacement curves are also found to agree with FEM results in Case I, as shown in Fig. 9g-9h.

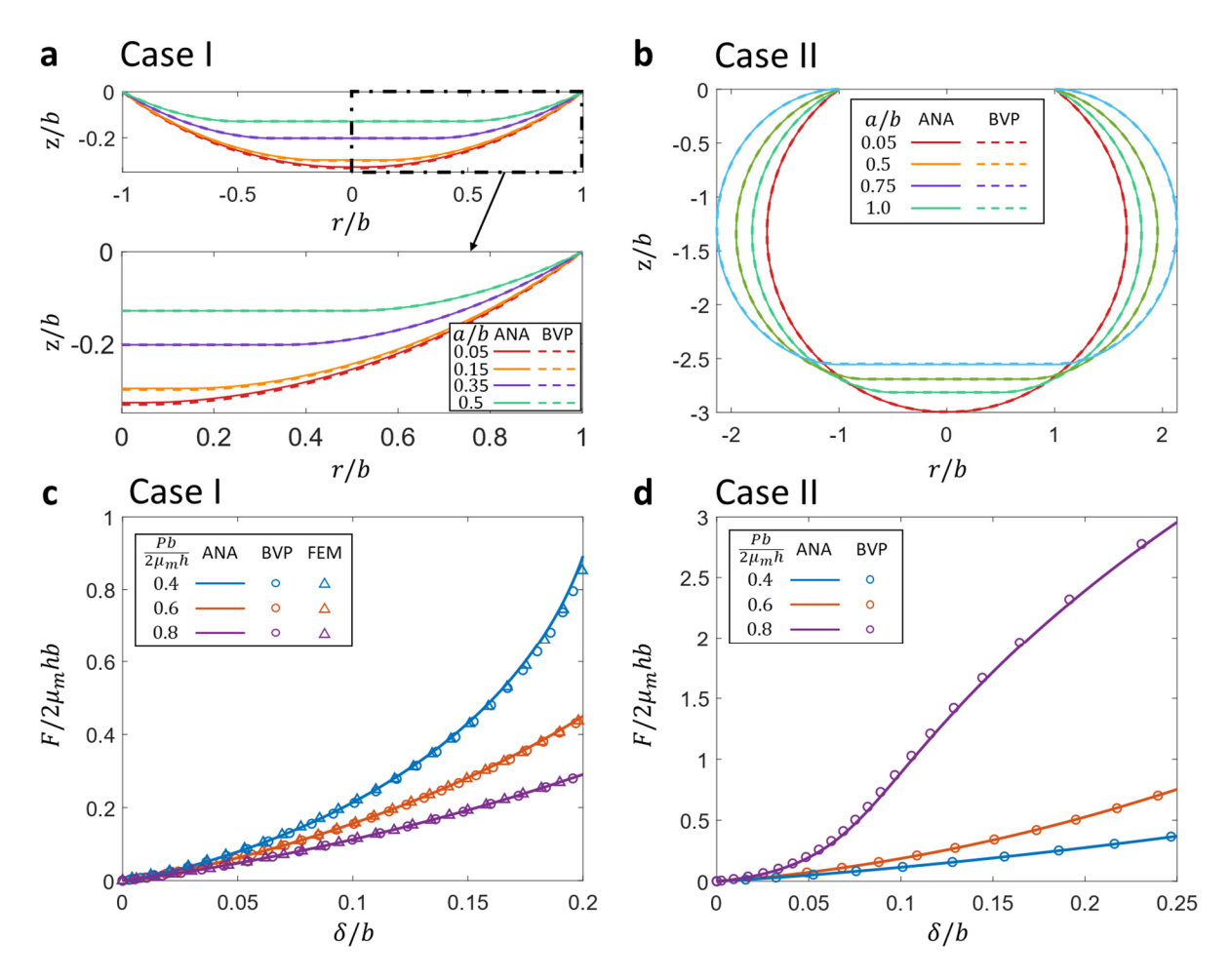


Figure 8 Inflated membrane in contact with flat rigid substrate with and $\lambda_0=2$. (a-b) Deformation profiles of the membrane with $Pb/2\mu_mh=1/\bar{R}=0.6$ and different contact radius (analytical: solid lines; BVP: dashed lines). The bottom inset in (a) shows a zoomed-in view of the membrane. (c-d) Normalized contact force $F/2\mu_mhb$ versus contact displacement δ/b under three different normalized pressure $Pb/2\mu_mh=0.4, 0.6$ or 0.8.

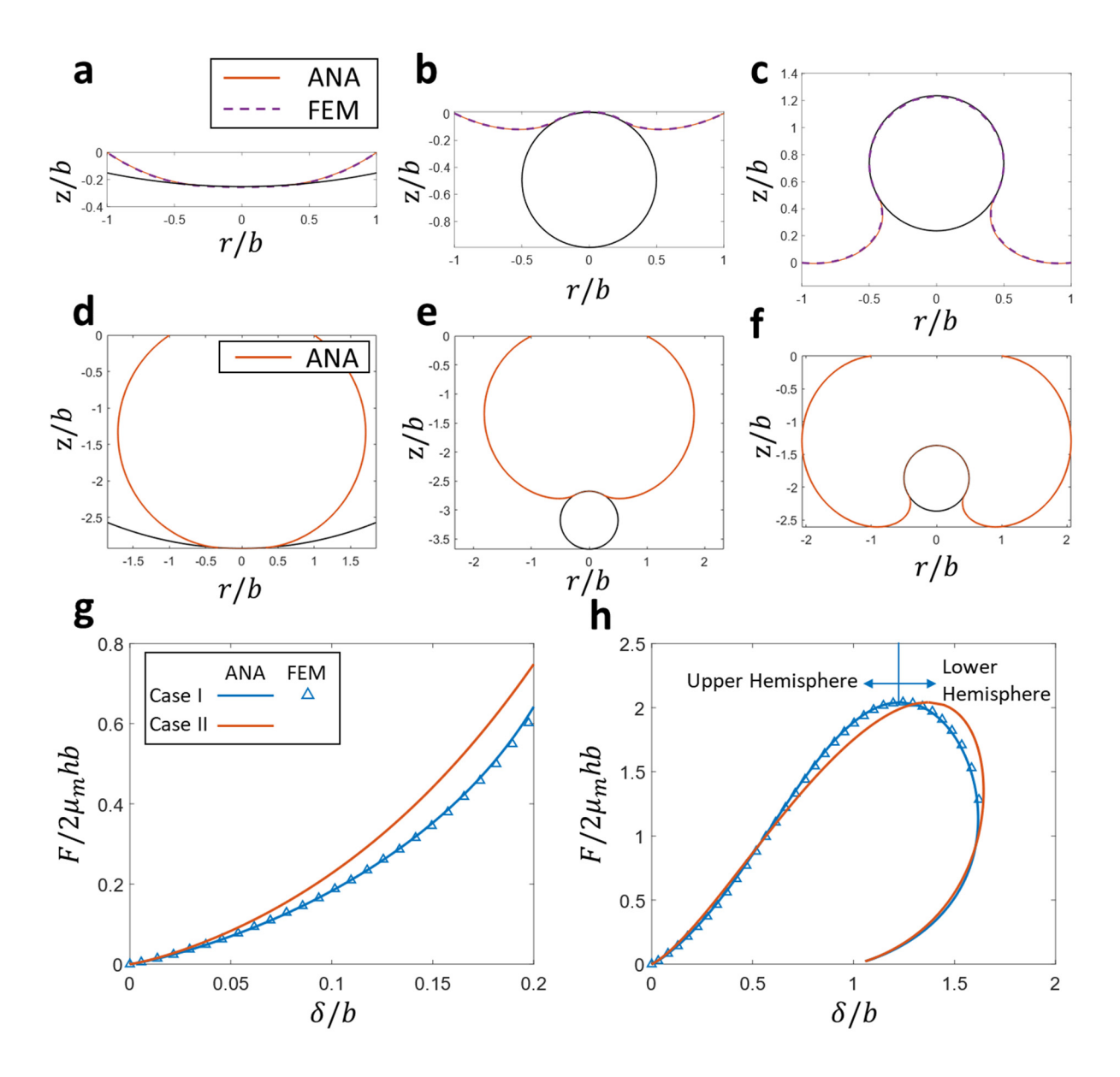


Figure 9 Inflated membrane in contact with spherically curved substrate with $\lambda_0 = 2$ and $Pb/2\mu_m h = 1/\bar{R} = 0.6$. (a-c) Deformation profiles of the membrane in Case I. (d-f) Deformation profiles of the membrane in Case II. (a) and (d): concave substrate with Rs/b = -5 and a/b = 0.329. (b) and (e): convex substrate with contact on the upper hemisphere with Rs/b = 0.5 and a/b = 0.25. (c) and (f): convex substrate with contact extended to the lower hemisphere with Rs/b = 0.5, a/b = 0.437. (g-h) Normalized contact force $F/2\mu_m hb$ versus contact displacement 8/b for concave and convex substrate, respectively.

3.4 Discussion: contact with convex substrate

The F versus δ curves for convex substrate in Fig.9h deserve a separation discussion. Unlike the flat or concave substrate, the F- δ curve for convex substrate, either in Case I or Case II, is non-monotonic and features a maximum in F and a maximum in δ . To understand this behavior, we first recall that F is directly proportional to the square of the contact radius a, as suggested by eq. (44). Normally a, defined as the radial coordinate at the contact edge (i.e., projection of the contact edge to the r-axis), increases as the contact area A expands, which is the case for the flat or concave substrate. For convex substrate, a cannot exceed the radius R_{δ} of the convex substrate and starts to decrease once the contact area A extends to the lower hemisphere. This behavior indicates that A is a more suitable metric to evaluate the expansion of contact region for convex substrates. Since the contact region is a spherical cap, we can write

$$a = \sqrt{\frac{A}{\pi} - \frac{A^2}{4\pi^2 R_s^2}} \ . \tag{57}$$

Equations (44) and (57) suggest that $F \sim a^2$ is a quadratic function of A that maximizes at $A = 2\pi R_s$, i.e., when the contact region covers the entire upper hemisphere and is about to extend to the lower hemisphere, as shown in Fig. 10a. This result explains the maximum F in Fig.9h.

On the other hand, the dependence of δ on a or A is much more complicated (see eq. (47) and (52) for Case I and eq. (48) and (56) for Case II). We plot δ as a function of A in Fig.10a using an example where $Pb/2\mu_m h = 0.6$. It is interesting to see that δ first increases with A and then maximizes at a point after the peak force F_m is achieved, which is consistent with the F- δ curves in Fig.9h. In a displacement-controlled contact process, the branch of solution after the peak displacement δ_m is not accessible. For example, our FEM results, shown as triangular symbols in Fig.10a, match well with the analytical solution before the peak displacement δ_m , but cannot provide any data after δ_m . In contrast, our analytical solutions can still capture the solution when A exceeds the point of peak displacement (see dashed lines in Fig.10a). To further understand the peak displacement δ_m , we plot the membrane profiles at three different contact area A for Case I (Fig.10c-10e) and Case II (Fig.10f-10h) of lower hemisphere contact. As A is increased, although the convex substrate indents more into the inflated membrane, the deflection of the free standing membrane given by -z(r=a) becomes larger, which effectively moves the convex substrate downwards and is attributed to the decreasing contact force F. Competition between these two

mechanisms results in a minimum in the total deflection $d \equiv -z(r=0)$ and hence a maximum in the contact displacement $\delta = d_0 - d$. Although Fig.10a shows that the peak displacements δ_m in Case I and Case II are close to each other, we emphasize that this result is not general. In Fig.10b, we plot δ versus A using an internal pressure of $Pb/2\mu_m h = 0.4$, showing distinct results for Case I and Case II. Moreover, the inset of Fig.10b shows that the peak displacement δ_m varies with the internal pressure P in Case I and Case II.

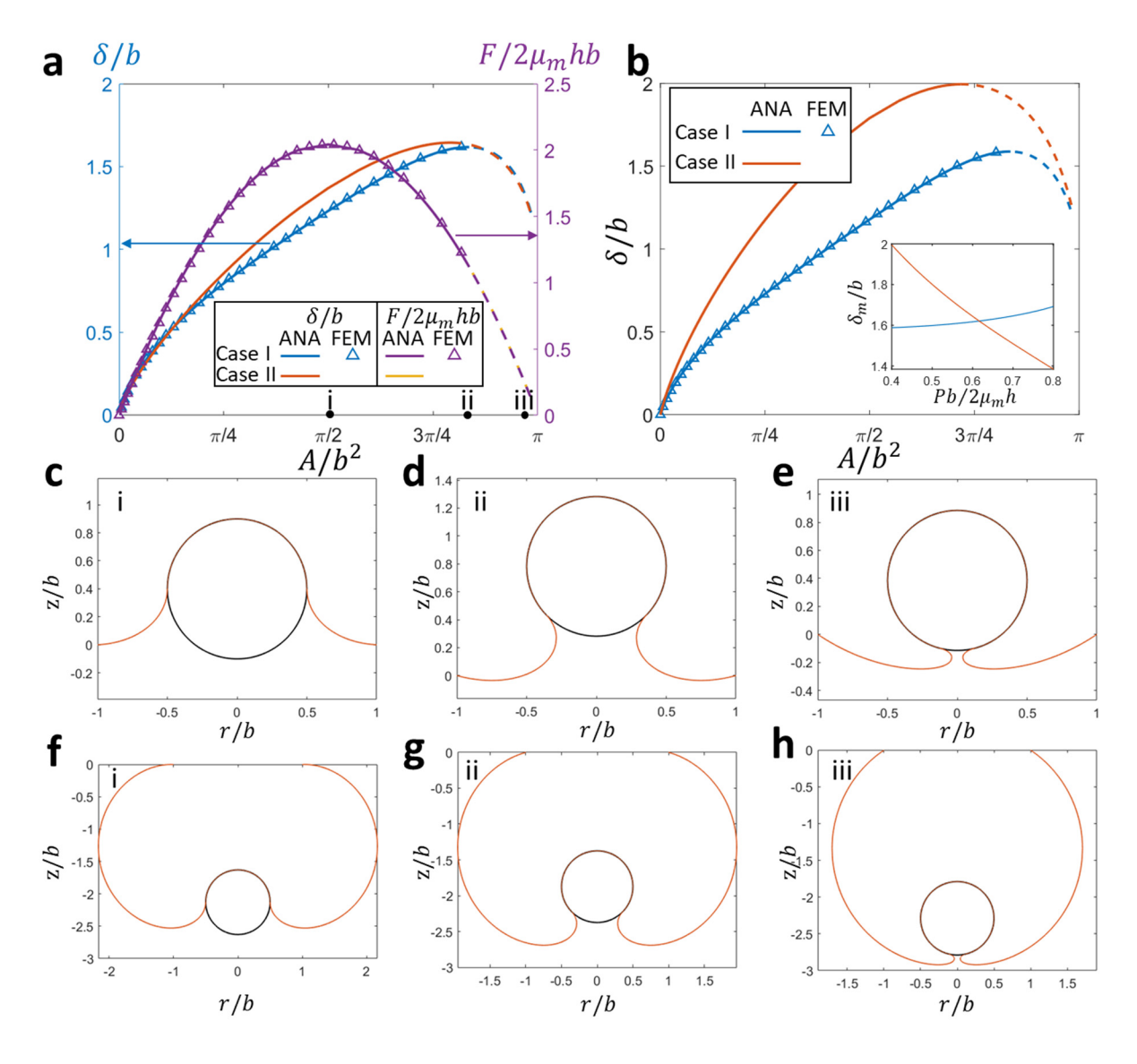


Figure 10 Contact with convex substrate. (a) Normalized contact force $F/2\mu_m hb$ and contact displacement δ/b versus contact area A/b^2 for $Pb/2\mu_m h=0.6$ and $R_s/b=0.5$. (b) Normalized contact displacement δ/b versus contact area A/b^2 for $Pb/2\mu_m h=0.4$ and $R_s/b=0.5$. The inset shows the normalized peak contact displacement δ/b versus normalized pressure $Pb/2\mu_m h$. (c-

e) Case I and (f-h) Case II membrane deformation profiles for lower hemipshere contact with i. a/b = 0.5, ii. a/b = 0.36, and iii. a/b = 0.125 for $Pb/2\mu_m h = 0.6$ and $R_s/b = 0.5$.

Figure 9h shows that the contact force F approaches 0 when the normalized contact displacement δb approaches 1. Recall that the solutions in Fig.9h are for the convex substrate with a radius $R_s/b = 0.5$. The limit of $\delta/b = 1$ corresponds to $\delta = 2R_s$, i.e., the contact displacement is equal to the diameter of the convex substrate. In this limit, the entire substrate sphere is wrapped by the membrane with a contact area of $A = 4\pi R_s^2$ (i.e., $A/b^2 = \pi$ since $R_s/b = 0.5$). The corresponding contact force F is zero, because the contact pressure P_e between the membrane and the substrate sphere is self-balanced and thus does not produce a net contact force. Figure 11a and 11b show nearly complete wrap of the substrate by the membrane given by Case I and Case II solutions, respectively. Note that complete wrap of the substrate sphere by the membrane would result in an infinite bending curvature at the bottom of the sphere, as illustrated in Fig.11c-11f showing zoomed-in views at the bottom of the sphere. Mathematically such severe curvature is allowed by the hyperelastic membrane theory, since it neglects bending rigidity of the membrane. However, resistance to bending would always emerge, even for thin membranes, when the curvature is sufficiently large. Therefore, complete wrap of the substrate sphere by the membrane is unlikely to occur in practice. As the configuration of complete wrapping is approached, we expect that the transition from stretching to bending should occur locally near the contact edge and such transition depends on the thickness of the membrane (Long et al., 2010). The competition between bending and stretching for nearly complete wrapping is beyond the scope of this work and is not pursued here.

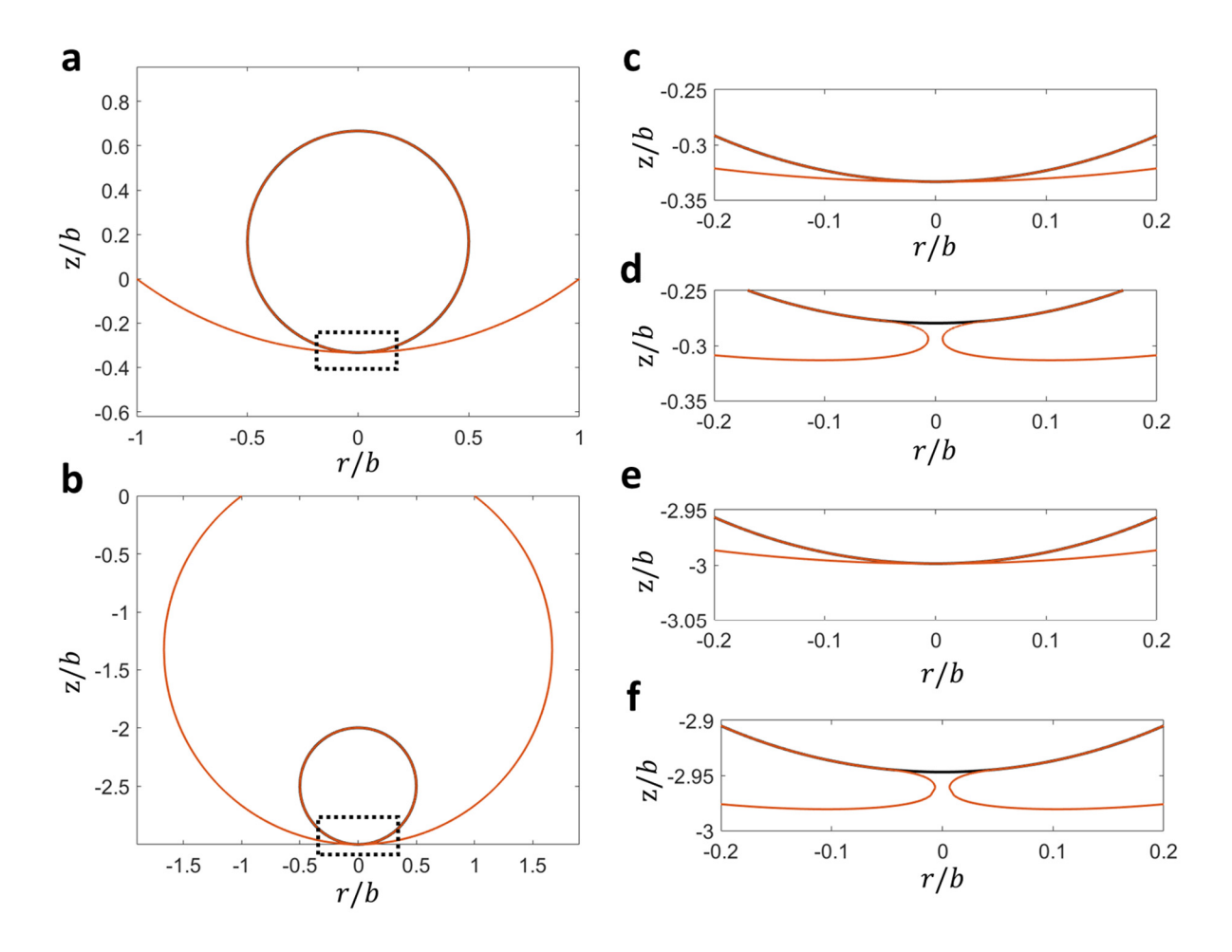


Figure 11 Deformed membrane profiles for contact with convex substrate. (a) Case I and (b) Case II solutions for lower hemisphere contact with a/b = 0.0005, $Pb/2\mu_m h = 0.6$ and $R_s/b = 0.5$. (c-f) Zoomed-in view of the membrane deformation near the bottom of the substrate for $Pb/2\mu_m h = 0.6$ and $R_s/b = 0.5$: (c-d) Case I with a/b = 0.0005 or 0.05, respectively; (e-f): Case II with a/b = 0.0005 or 0.05, respectively.

4. Contact with an elastic substrate

In this section, we present analytical solutions for the inflated membrane in contact with an elastic substrate. Similar to Section 3, we will first consider flat elastic substrates (Section 4.1) and then extend the solutions to spherically curved elastic substrates (Section 4.2). Validation of the analytical solutions using FEM results will be shown in Section 4.3.

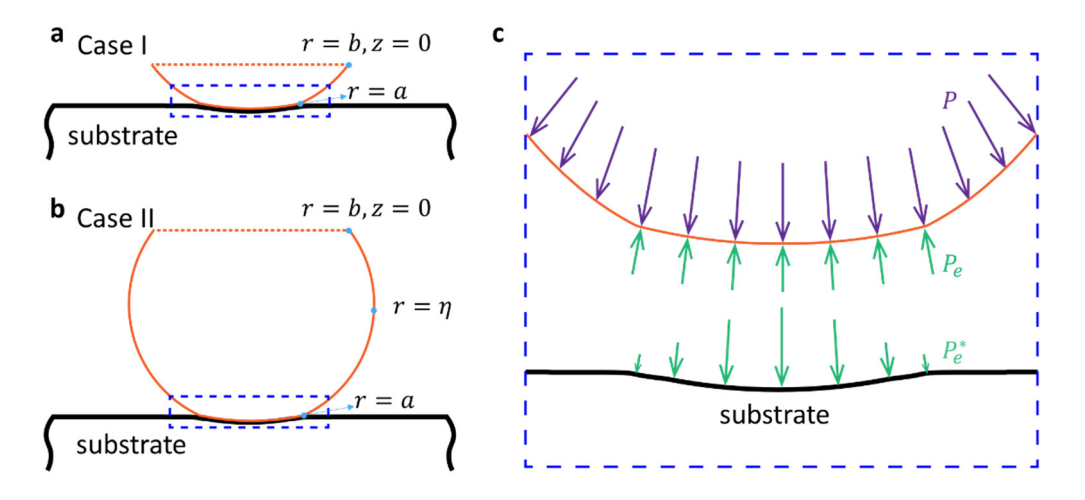


Figure 12 Schematics of the inflated membrane in contact with a flat elastic substrate. (a) Case I. (b) Case II. (c) A zoomed-in view of the contact region showing the pressure on the membrane and the substrate, where P is the internal pressure within the membrane, P_e^* is the distributed Hertz contact pressure on the substrate, and P_e is the approximated uniform contact pressure on the membrane.

4.1 Contact with a flat elastic substrate

The substrate is assumed to be an elastic half-space with Young's modulus E_s and Poisson's ratio v_s . Upon contact with the inflated membrane, both the membrane and substrate deform as shown in Fig.12a and 12b. If exact solutions are sought, one would need to solve the unknown distribution of contact pressure by writing the surface displacement profile of the substrate through the Green's function approach and setting it equal to the membrane profile due to conformal contact. However, this would result in an integral equation that is unsolvable analytically. To obtain analytical solutions, we simplify the problem by approximating the contacting membrane as a spherical cap with radius R^* . To be consistent with the sign convention of free inflation radius R, we let R^* be positive if the contacting membrane is convex and negative if otherwise. For the flat elastic substrate, we expect R^* to be positive (see Fig.12c) because the substrate cannot bulge up under adhesionless contact. Similar to Section 3.2, the spherical cap profile of the contacting membrane implies that it is subjected to a uniform internal pressure P and a uniform contact pressure P_e (see Fig.12c). The radius R^* satisfies the following equation:

$$\frac{2\mu_{m}h}{R^{*}} = P - P_{e} \,. \tag{58}$$

Because $P - P_e < P$, we expect R^* to be larger than the free inflation radius $R = 2\mu_m h/P$. Given that both R^* and P_e are unknown, we need to consider deformation in the elastic substrate. The substrate is effectively indented by a rigid sphere with radius R^* with no adhesion and friction. Therefore, we utilize the Hertz contact theory which gives the following distribution of contact pressure in the contact region

$$P_e^*(r) = \frac{3F}{2\pi a^2} \left(1 - \frac{r^2}{a^2} \right)^{1/2},\tag{59}$$

where a is the contact radius and F is the compressive contact force. The contact force F is given by

$$F = \frac{4E_s^* a^3}{3R^*},\tag{60}$$

where $E_s^* = E_s / (1 - v_s^2)$ is the plane strain modulus of the substrate. Apparently, the contact pressure P_e^* on the substrate is not uniform, which contradicts the uniform contact pressure P_e on the membrane. This discrepancy implies that the contacting membrane should not exactly have a spherical shape. As an approximation, we set P_e to be the average value of the Hertzian contact pressure P_e^* :

$$P_e \approx \frac{F}{\pi a^2} = \frac{4E_s^* a}{3\pi R^*} \,. \tag{61}$$

Effectively, we assume that deformation of the contacting membrane can be approximated to the first order by retaining the spherical shape but allowing its radius R^* to change. Combining eq. (58) and (61), we obtain:

$$\frac{R}{R^*} = \frac{1}{1 + \frac{2E_s^* a}{3\pi \mu_m h}},\tag{62}$$

where we have used the free inflation radius $R = 2\mu_m h/P$. Introducing a dimensionless parameter

$$\gamma = \frac{3\pi\mu_m h}{2E_s^* a},\tag{63}$$

we can rewrite eq. (62) as

$$\frac{R}{R^*} = \frac{\gamma}{1+\gamma} \,. \tag{64}$$

Physically, γ represents the competition between the stiffness of the inflated membrane and that of the substrate. The limit of $\gamma = 0$ recovers the case of flat rigid substrate. In the limit of γ approaching $+\infty$, the Hertz contact problem of a rigid sphere with radius R (i.e., the inflated membrane) on an elastic half space is recovered.

With the approximation described above, the membrane deformation can be calculated using the same solutions as those for the spherically curved rigid substrates (Section 3.2). Specifically, the contacting membrane is under biaxial stretch and its spherical profile implies that the tangent angle θ_0 at the contact edge is given by

$$\sin \theta_0 = \frac{a}{R^*} \text{ at } r = a. \tag{65}$$

Following the definition of ζ in eq. (32), we have

$$\zeta = \frac{R\sin\theta_0}{a} = \frac{R}{R^*} = \frac{\gamma}{1+\gamma},\tag{66}$$

where one can show that $0 < \zeta < 1$ because $\gamma > 0$. It should be noted the definition of ζ here (i.e., $= R/R^*$) is similar to that for the spherically curved rigid substrate (i.e., $\zeta = -R/R_s$) where the extra "—" sign is due to the different sign convention for R_s and R^* . By substituting ζ in eq. (66) into eq. (34) and (35), we can calculate the deformation profiles of the free standing membrane, as detailed below.

Case I: deformation profile of the free standing membrane is given by eq. (36). Unlike the rigid substrates, here the vertical gap d between the fixed edge of the membrane and the substrate is equal to the total deflection, -z(r=0), subtracted by Hertzian indentation depth of the substrate which is equal to a^2/R^* , i.e.,

$$d = -z(r=0) - \frac{a^2}{R^*} = b\Phi(b; \overline{a}, \overline{R}, \zeta) + R^* - \sqrt{R^{*2} - a^2} - \frac{a^2}{R^*}.$$
 (67)

Accordingly, the contact displacement δ is

$$\delta = d_0 - d = R - \sqrt{R^2 - b^2} - b\Phi(b; \overline{a}, \overline{R}, \zeta) - R^* + \sqrt{R^{*2} - a^2} + \frac{a^2}{R^*}.$$
 (68)

Case II: deformation profile of the free standing membrane is given by eq. (41) and (42) with the critical point η given by eq. (39). Similar to Case I, the vertical gap d is given by

$$d = -z(r=0) - \frac{a^2}{R^*} = 2b\Phi(\eta; \overline{a}, \overline{R}, \zeta) - b\Phi(b; \overline{a}, \overline{R}, \zeta) + R^* - \sqrt{R^{*2} - a^2} - \frac{a^2}{R^*}.$$
 (69)

The contact displacement δ is therefore

$$\delta = d_0 - d = R + \sqrt{R^2 - b^2} - 2b\Phi(\eta; \overline{a}, \overline{R}, \zeta) + b\Phi(b; \overline{a}, \overline{R}, \zeta) - R^* + \sqrt{R^{*2} - a^2} + \frac{a^2}{R^*}.$$
 (70)

For both cases, the contact force F is given by eq. (60). By combining eq. (58), (61) and (62), the contact force F can also be casted in the form of eq. (44) with ζ given by eq. (66).

4.2 Contact with a spherically curved elastic substrate

We extend the solutions in Section 4.1 to account for scenarios where the substrate is elastic and spherically curved with radius R_s . The center of the spherical substrate is located on the z-axis (i.e., the axis of symmetry). The sign convention of R_s is the same as that in Section 3.2: $R_s < 0$ if the substrate is concave and $R_s > 0$ if the substrate is convex. We apply the same approximation as in Section 4.1 that the contacting membrane has a spherical profile with radius R^* . To apply the Hertz theory, we introduce the combined radius R':

$$\frac{1}{R'} = \frac{1}{R^*} + \frac{1}{R_s} \,. \tag{71}$$

Using the combined radius, the contact force F given by the Hertz theory becomes:

$$F = \frac{4E_s^* a^3}{3R'},\tag{72}$$

By combining eq. (58) and (72) and using $P_e \approx F/\pi a^2$, we obtain that

$$\zeta = \frac{R}{R^*} = \frac{1}{1+\gamma} \left(\gamma - \frac{R}{R_s} \right). \tag{73}$$

Following the same reasoning in Section 4.1, we can calculate the deformation profiles of the free standing membrane using eq. (34) and (35) with ζ defined in eq. (73). For concave substrates, R_s < 0 and we require $R < |R_s|$ to prevent the formation of annular contact region. Given that $\gamma > 0$, one can show that $0 < \zeta < 1$. For convex substrates, $R_s > 0$ and one can show that $\zeta < 1$ but ζ may become negative if $\gamma < R/R_s$. Since eq. (73) is the most general definition of ζ , we can recover to the scenarios discussed in previous sections. If the substrate is rigid, we have $\gamma = 0$ and $\zeta = -R/R_s$, which recovers the scenarios with rigid substrates in Section 3. If the substrate is flat and elastic, we have $R_s = \pm \infty$ and $\zeta = \gamma/(1+\gamma)$, which recovers eq. (66) in Section 4.1.

It should be emphasized that the Hertz contact theory assumes linear elasticity and infinitesimal deformation in the substrate and thus is limited to the regime with small contact radius (e.g., $a \ll |R_s|$). Consequently, we do not consider the membrane contact with the lower hemisphere of the elastic convex substrate as in Section 3.2.3. Next, we summarize the solutions for membrane deformation profiles for Case I and II.

Case I: deformation profile of the free standing membrane is given by eq. (36) using ζ in eq. (73). The vertical gap d is given by

$$d = b\Phi(b; \overline{a}, \overline{R}, \zeta) + sign(R^*) \left(\left| R^* \right| - \sqrt{R^{*2} - a^2} \right) - \frac{a^2}{R'}, \tag{74}$$

where the absolute value on R^* is to accommodate the possibility that R^* can be negative, and a^2/R' is the Hertz indentation depth of the curved substrate. The contact displacement δ is

$$\delta = d_0 - d = R - \sqrt{R^2 - b^2} - b\Phi(b; \overline{a}, \overline{R}, \zeta) - sign(R^*) (|R^*| - \sqrt{R^{*2} - a^2}) + \frac{a^2}{R'}.$$
 (75)

Case II: deformation profile of the free standing membrane is given by eq. (41) and (42) with the critical point η given by eq. (39) and ζ in eq. (73). The vertical gap d is

$$d = 2b\Phi(\eta; \overline{a}, \overline{R}, \zeta) - b\Phi(b; \overline{a}, \overline{R}, \zeta) + sign(R^*)(|R^*| - \sqrt{R^{*2} - a^2}) - \frac{a^2}{R'}.$$
 (76)

The contact displacement δ is:

$$\delta = R + \sqrt{R^2 - b^2} - 2b\Phi(\eta; \overline{a}, \overline{R}, \zeta) + b\Phi(b; \overline{a}, \overline{R}, \zeta) - sign(R^*)(|R^*| - \sqrt{R^{*2} - a^2}) + \frac{a^2}{R'}. \quad (77)$$

For both cases, the contact force is given by eq. (72) and can be casted in the form of eq. (44) with ζ given by eq. (73).

4.3 Validation using FEM results

To validate the analytical solutions for elastic substrates, we use the FEM model described in Section 3.3 to perform simulations where the Young's modulus E_s of the substrate is varied to show the effect of γ . Again, only Case I results are obtained from the FEM.

Figures 13, 14 and 15 show the membrane deformation profiles (Case I and II) as well as the corresponding contact force F versus displacement δ curves for the flat, concave and convex elastic substrates, respectively. FEM results for Case I are also plotted in these figures for comparison. Because the dimensionless parameter γ decreases as the contact radius a increases (see eq. (63)), it is not a constant during the contact process. Therefore, instead of prescribing γ , we vary $\mu_m h/E_s^* b$ in Fig.13-15 which is related to γ through

$$\frac{\mu_m h}{E_b^* b} = \frac{2\gamma}{3\pi} \frac{a}{b} \,. \tag{78}$$

Since a/b < 1, $\mu_m h/E_s^*b$ can be interpreted as the lower bound of $2 \not / 3\pi$. In all three figures, our analytical solutions for Case I of the membrane deformation profile agree well with the FEM results. For the F versus δ curves, we use red lines to represent the limit of small $\mu_m h/E_s^*b$, i.e., very stiff substrate, and green lines to represent the limit of large $\mu_m h/E_s^*b$, i.e., very soft substrate. In the former limit (stiff substrate), we recover the scenario of rigid substrate contact, and our analytical solutions show good agreement with FEM results across a large range of displacement (see red solid lines and symbols in Fig.13c, 14c and 15c). This is expected because the large stretch approximation in eq. (8) is accurate when we included a pre-stretch ($\lambda_0 = 2$). In the latter limit (soft substrate), we expect the inflated membrane does not further deform upon contact and acts as a rigid indenter on the substrate, i.e., the Hertz contact problem is recovered. Our analytical solutions for the F versus δ curve agree well with the FEM results at relatively small δ but exhibit larger discrepancy as δ is increased (see green solid lines and symbols in Fig.13c, 14c and Fig. 15c). Relative to the flat substrate, such discrepancy is larger for the concave substrate ($R_s/b = -5$) and significantly reduced for the convex substrate ($R_s/b = 0.5$). We attribute the discrepancy to the fact

the Hertz contact theory employed in our analytical solutions is valid for small contact radius. As the contact radius is increased, the Hertz theory becomes less accurate. The reduced discrepancy observed for the convex substrate ($R_s/b = 0.5$) is because under the same contact displacement δ , the convex substrate features a smaller contact radius as compared to the concave or the flat substrate, which improves the accuracy of the Hertz contact theory.

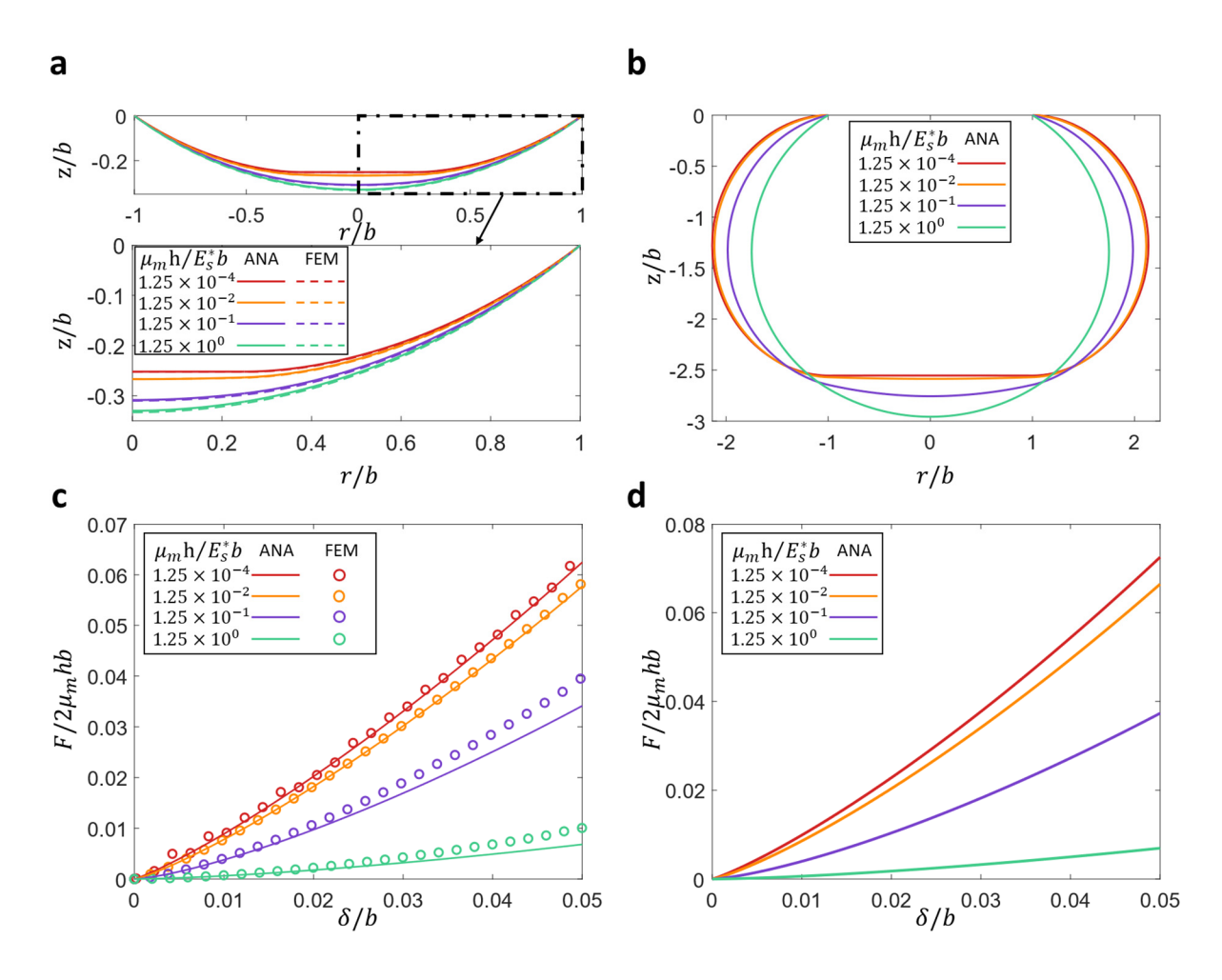


Figure 13 Inflated membrane in contact with a flat elastic substrate with $Pb/2\mu_m h = 0.6$ and $\lambda_0 = 2$. (a-b) Deformation profiles of the membrane for (a) Case I with a/b = 0.25 and (b) Case II with a/b = 1. The bottom inset in (a) shows a zoomed-in view of the membrane. (c-d) Normalized contact force $F/2\mu_m hb$ versus contact displacement δ/b for (c) Case I and (d) Case II.

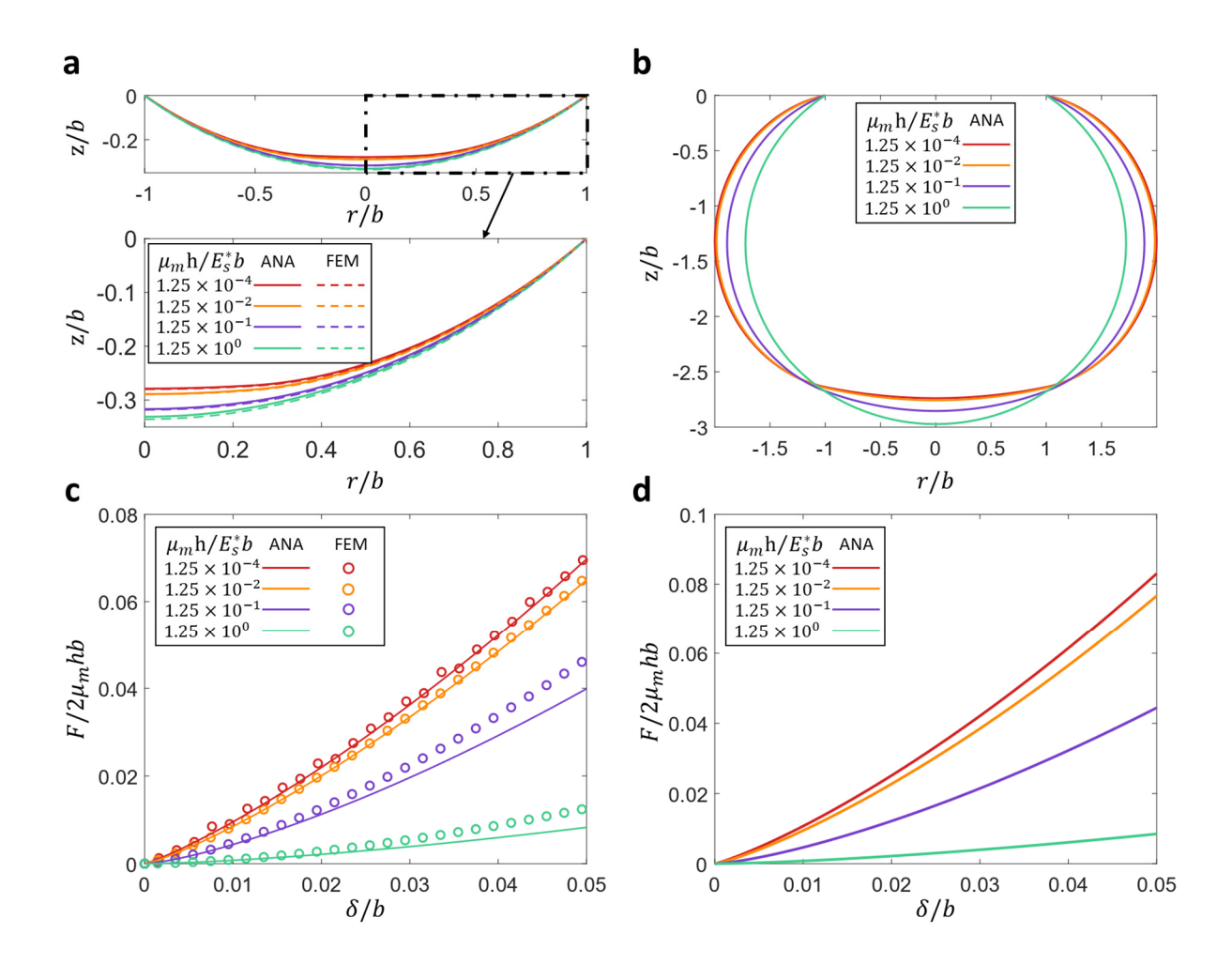


Figure 14 Inflated membrane in contact with a concave elastic substrate with $R_s/b = -5$, $Pb/2\mu_m h$ = 0.6 and $\lambda_0 = 2$. (a-b) Deformation profiles of the membrane for (a) Case I with a/b = 0.25 and (b) Case II with a/b = 1. The bottom inset in (a) shows a zoomed-in view of the membrane. (c-d) Normalized contact force $F/2\mu_m hb$ versus contact displacement δ/b for (c) Case I and (d) Case II.

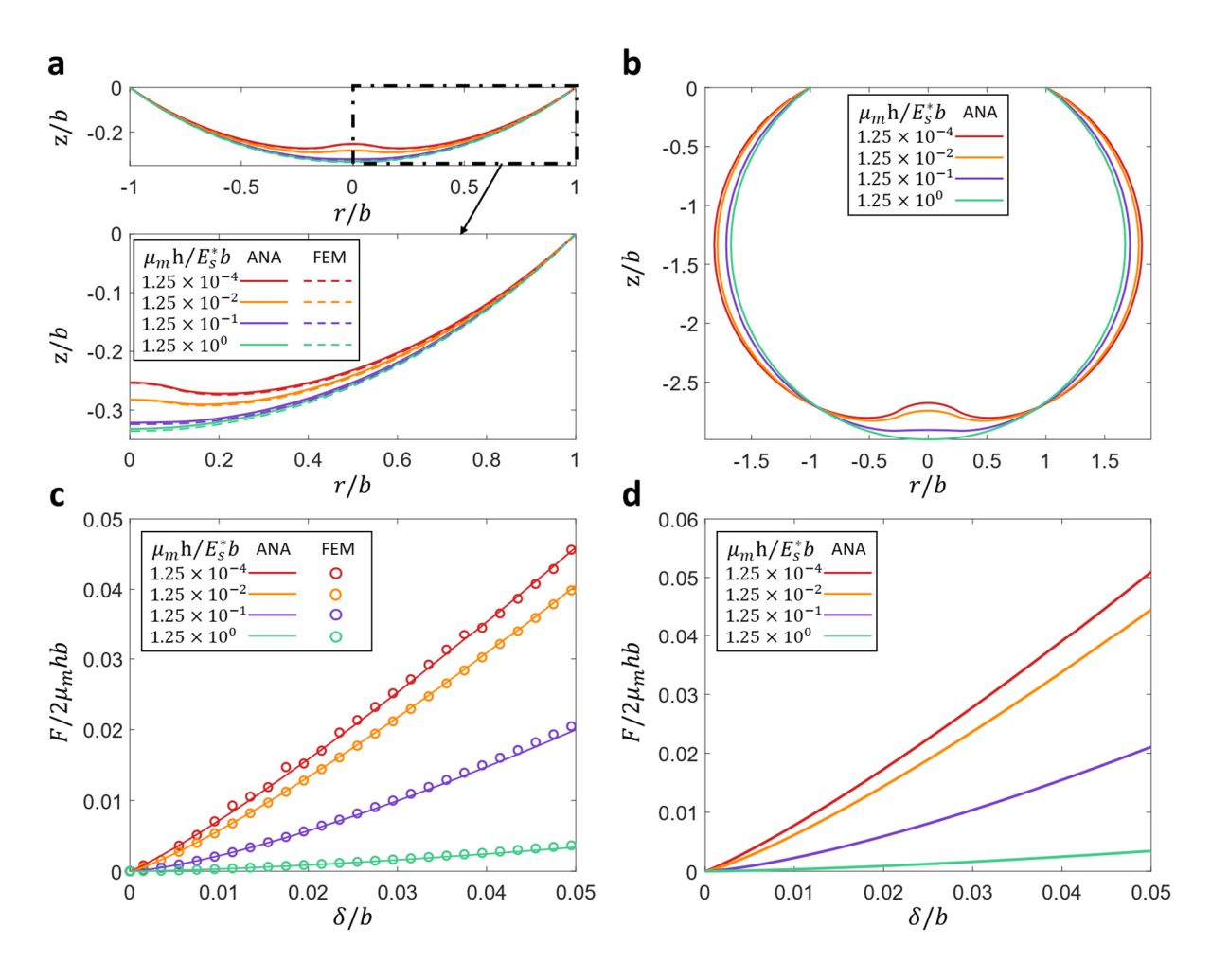


Figure 15 Inflated membrane in contact with a convex elastic substrate with $R_s/b = 0.5$, $Pb/2\mu_m h = 0.6$ and $\lambda_0 = 2$. (a-b) Deformation profiles of the membrane for (a) Case I with a/b = 0.1 and (b) Case II with a/b = 0.25. The bottom inset in (a) shows a zoomed-in view of the membrane. (c-d) Normalized contact force $F/2\mu_m hb$ versus contact displacement δ/b for (c) Case I and (d) Case II.

6. Conclusion

We present analytical solutions of an axisymmetric inflated neo-Hookean membrane in frictionless and adhesionless contact with various types of substrates. Following the approach of Foster (1967a, 1967b) we used the large stretch approximation for neo-Hookean membrane to obtain a general analytical solution for the axisymmetric membrane under uniform pressure. Using this solution, we first showed that under free inflation, the originally flat membrane deforms to a spherical cap with a radius *R* that is inversely proportional to the pressure *P*. There are two cases of solutions associated with the same pressure which are referred to as Case I and Case II. By

combining the analytical solution of free standing membrane and boundary conditions dictated by the geometry of the contacting membrane, we obtained analytical solutions for the membrane in contact with flat rigid and spherically curved rigid substrates. In case of elastic substrates, by introducing an approximation where the contact membrane is in the shape of a spherical cap and combining the membrane solution with the Hertz contact theory, we obtained analytical solutions for the membrane in contact with flat elastic and spherically curved elastic substrates. In particular, we found a dimensionless parameter γ that captures the transition between two limiting cases, i.e., either the substrate or the inflated membrane is effectively rigid relative to the other component and thus experiences negligible deformation upon contact. The analytical solutions were validated against numerical solutions of Long et al. (2010) for the free inflation and the contact with flat rigid substrate, where excellent agreement was found under sufficient pre-stretch. FEM simulations were used to validate the Case I analytical solutions for the contact with flat rigid, spherically curved rigid, flat elastic, and spherically curved elastic substrates, where good agreement was also found. While our solutions for the rigid substrate are valid for the entire range of contact radius, our solutions for the elastic substrate are valid for small contact radius due to limitation of the Hertz contact theory.

The closed-form but approximate analytical solutions for inflated membrane contact presented in this paper cover a large range of substrate geometry and stiffness. Although these analytical solutions are approximate in nature, they can be useful for efficiently exploring the parametric space of operation and design in applications such as soft pneumatic actuators and haptic transducers, especially for membranes undergoing large deformation with multiple solutions and bifurcation (Liu et al., 2021).

Acknowledgements

The authors acknowledge funding support from the National Science Foundation through a CAREER award (NSF CMMI-1752449).

Appendix A: Derivation of eq. (9)

We first substitute eq. (5) into eq. (4) and utilize eq. (6) to obtain:

$$\frac{d\left(T_{1}r\sin\theta\right)}{dr} = Pr. \tag{A1}$$

If the applied pressure P is uniform, eq. (A1) can be integrated to give

$$T_1 r \sin \theta = \frac{P(r^2 + C_1)}{2},\tag{A2}$$

where C_1 is an integration constant that needs to be determined by boundary conditions.

Substituting eq. (A2) and (8) into eq. (4) results in the following equation:

$$\frac{P(r^2 + C_1)}{2r\sin\theta} \frac{d\theta}{d\xi} + \frac{2\mu_m^2 h^2}{P(r^2 + C_1)} \sin^2\theta = P.$$
 (A3)

To further integrate eq. (A3), we cast it into the following form using eq. (6):

$$\frac{P(r^2 + C_1)}{2r\sin\theta} \frac{d\theta}{dr} \cos\theta + \frac{2\mu_m^2 h^2}{P(r^2 + C_1)} \sin^2\theta = P, \qquad (A4)$$

which can be further changed to

$$-\frac{P(r^2 + C_1)}{4r\sin^2\theta} \frac{d\cos^2\theta}{dr} + \frac{2\mu_m^2 h^2}{P(r^2 + C_1)} \sin^2\theta = P.$$
 (A5)

Next, we apply a change of variable that $\beta = 1 - \cos^2 \theta = \sin^2 \theta$, which gives

$$\frac{P(r^2+C_1)}{4r\beta}\frac{d\beta}{dr} + \frac{2\mu_m^2 h^2}{P(r^2+C_1)}\beta = P.$$
(A6)

To integrate eq. (A6), we first rearrange it to

$$-\frac{P(r^2+C_1)}{4r}\beta\frac{d(1/\beta)}{dr} + \frac{2\mu_m^2 h^2}{P(r^2+C_1)}\beta = P,$$
 (A7)

which can be written as

$$2r\mu_m^2 h^2 = P^2 r \left(r^2 + C_1\right) \frac{1}{\beta} + \frac{P^2 \left(r^2 + C_1\right)^2}{4} \frac{d\left(1/\beta\right)}{dr}.$$
 (A8)

Combining the two terms on the right hand side of eq. (A8), we obtain

$$2r\mu_m^2 h^2 = \frac{d}{dr} \left[\frac{P^2 \left(r^2 + C_1 \right)^2}{4} \frac{1}{\beta} \right]. \tag{A9}$$

Integration of eq. (A9) gives

$$\frac{P^2 \left(r^2 + C_1\right)^2}{4} \frac{1}{\beta} = \mu_m^2 h^2 r^2 + C_2, \tag{A10}$$

where C_2 is another integration constant. Substituting $\beta = \sin^2 \theta$ in eq. (A7), we arrive at eq. (9) in the main text.

Appendix B: Analytical solution for free inflation

At the apex of the membrane (r = 0), symmetry dictates that the membrane is flat and subjected to biaxial tension, i.e.,

$$\theta = 0$$
 and $\lambda_1 = \lambda_2$ at $r = 0$, (B1)

The former condition ($\theta = 0$ at r = 0) and eq. (A2) imply that $C_1 = 0$. The latter condition ($\lambda_1 = \lambda_2$ at r = 0) and eq. (8) result in that

$$T_1 = T_2 \approx \mu_m h \text{ at } r = 0.$$
 (B2)

Using eq. (B2) and comparing eq. (A2) and (9), we conclude that $C_2 = 0$. Therefore, we have

$$\sin \theta = \frac{P}{2\mu_m h} r \,, \tag{B3}$$

where we have used the range $0 \le \theta \le \pi$ so that $\sin \theta \ge 0$. Using eq. (B3) and the identity that $dz/dr = \tan \theta$, we have

$$dz = \tan\theta dr = \frac{2\mu_m h}{P} \sin\theta d\theta. \tag{B4}$$

Integrating eq. (B4) and applying the boundary condition at the fixed edge that

$$z = 0$$
 at $r = b$ (i.e., at $\sin \theta = \frac{Pb}{2\mu_m h}$), (B5)

we arrive at the following result:

$$z \pm \sqrt{\left(\frac{2\mu_m h}{P}\right)^2 - b^2} = \frac{2\mu_m h}{P} \cos\theta.$$
 (B6)

Combining eq. (B3) and (B6), we find that the deformation profile of the membrane is a spherical cap given by eq. (10).

The spherical geometry of an inflated membrane has a general implication that warrants discussion. If the deformed membrane has a spherical shape with a radius of R and is under a uniform pressure P, both of the two principal curvatures are equal to 1/R. Therefore, the equilibrium equation in eq. (4) becomes:

$$T_1 + T_2 = PR. (B7)$$

Substituting eq. (B7) into eq. (5) and we obtain

$$r\frac{dT_1}{dr} + 2T_1 = PR. (B8)$$

The general solution of eq. (B8) is

$$T_1 = \frac{PR}{2} + \frac{C_3}{r^2},\tag{B9}$$

where C_3 is an integration constant. Since T_1 must be finite at r=0, we have to set $C_3=0$, which means $T_1=T_2=PR/2=\mu_m h$. In other words, the spherical portion of the membrane must be under uniform equibiaxial tension. Combining this result with eq. (8), we conclude that $\lambda_1=\lambda_2$ throughout the spherical portion of the inflated membrane. Note that although $\lambda_1=\lambda_2$ throughout the spherical membrane, the value of the biaxial stretch (i.e., λ_1 or λ_2) is not necessarily uniform in the membrane, as pointed out by Foster (1967b). Specifically, Long et al. (2010) showed that under free inflation, the areal strain at the apex of the membrane can be much larger than that the average areal strain of the entire membrane. This feature, although counter-intuitive, is attributed to the fact that $T_1 \approx T_2 \approx \mu_m h$ for neo-Hookean membrane under large deformation as long as the

membrane is under equibiaxial stretch (i.e., $\lambda_1 = \lambda_2$), regardless of what values the stretch ratios are.

Appendix C: Representing the integral function in eq. (18) using elliptic integrals

Based on $\Psi(r; \bar{a}, \bar{R})$ in eq. (18), we implement a change of variable that $t = s^2 - a^2$ and obtain the following expression:

$$\Psi(r; \overline{a}, \overline{R}) = \frac{1}{b} \int_{a}^{r} \frac{\left(s^2 - a^2\right)}{\sqrt{R^2 s^2 - \left(s^2 - a^2\right)^2}} ds = \frac{1}{b} \int_{0}^{r^2 - a^2} \frac{t}{2\sqrt{a^2 R^2 + R^2 t - t^2}} \frac{1}{\sqrt{t + a^2}} dt. \quad (C1)$$

To proceed, we define the following parameters:

$$\alpha_2 = \frac{R^2 + R\sqrt{R^2 + 4a^2}}{2},\tag{C2}$$

$$\alpha_2 = \frac{R^2 - R\sqrt{R^2 + 4a^2}}{2},\tag{C3}$$

and

$$\alpha_3 = -a^2 \,. \tag{C4}$$

Using eq. (C2) - (C4), we can rewrite eq. (C1) as:

$$\Psi(r;\overline{a},\overline{R}) = \frac{1}{b} \int_{0}^{r^{2}-a^{2}} \frac{t}{2\sqrt{-(t-\alpha_{1})(t-\alpha_{2})(t-\alpha_{3})}} dt.$$
 (C5)

The integral on the right hand side of eq. (C5) is the same as eq. (64) in Foster (1967a), except that Foster normalized the integral variable. Given that $\alpha_1 > \alpha_1 > \alpha_1$ and $t = s^2 - a^2 < \eta^2 - a^2 = \alpha_1$ because the radial coordinate of the free standing membrane cannot exceed the critical point at $r = \eta$, we can write the following indefinite integral in terms of the elliptic integral according to eq. (65) in Foster (1967a):

$$\int \frac{t}{2\sqrt{-(t-\alpha_1)(t-\alpha_2)(t-\alpha_3)}} dt$$

$$= \frac{1}{\sqrt{\alpha_1-\alpha_3}} \left\{ \alpha_3 F(\varphi,k) + (\alpha_1-\alpha_3) E(\varphi,k) - \frac{(\alpha_1-\alpha_2)\sin\varphi\cos\varphi}{\sqrt{1-k^2\sin^2\varphi}} \right\} + C^*$$
(C6)

where C^* is an integration constant, $F(\varphi, k)$ and $E(\varphi, k)$ are the incomplete elliptic integral of the first and second kind, respectively. The variables in the elliptic integral, k and φ , are

$$k^2 = \frac{\alpha_1 - \alpha_2}{\alpha_1 - \alpha_3},\tag{C7}$$

$$\sin^2(\varphi) = \frac{\alpha_2 - t}{(\alpha_3 - t)k^2} \,. \tag{C8}$$

We denote the function on the right hand side of eq. (C6) as f(t), i.e.,

$$f(t) = \frac{1}{\sqrt{\alpha_1 - \alpha_3}} \left\{ \alpha_3 F(\varphi, k) + (\alpha_1 - \alpha_3) E(\varphi, k) - \frac{(\alpha_1 - \alpha_2) \sin \varphi \cos \varphi}{\sqrt{1 - k^2 \sin^2 \varphi}} \right\}.$$
 (C9)

Using eq. (C6) and (C9), we can write eq. (C5) as

$$\Psi(r;\overline{a},\overline{R}) = \frac{1}{b}f(r^2 - a^2) - \frac{1}{b}f(0) . \tag{C10}$$

Therefore, the integral function $\Psi(r; \bar{a}, \bar{R})$ in eq. (30) can be expressed in terms of incomplete elliptic integrals.

Appendix D: Comparison with the linear analysis by Xu and Liechti (2011)

Xu and Liechti (2011) considered the adhesionless contact between an inflated membrane and a flat rigid substrate assuming linear elasticity and small membrane deflection. Here we compare our solutions for free inflation and contact with flat rigid substrate with the corresponding solutions by Xu and Liechti (2011). Specifically, for free inflation, we adapt equation (10) in Xu and Liechti (2011) that relates the internal pressure, P, to the deflection at the apex of the membrane, d_0 :

$$\frac{P}{2\mu_{m}h} = \frac{6d_{0}^{3}}{b^{4}} + \frac{2\sigma_{0}d_{0}}{\mu_{m}b^{2}},\tag{D1}$$

where σ_0 is the equibiaxial tensile residual stress in the membrane. To connect eq. (D1) to our solutions, we note that in our problem the pre-stretched membrane is under an equibiaxial line tension of $T_1 = T_2 = \mu_m h$ due to the large stretch approximation, which corresponds to a residual stress of $\sigma_0 = T_1/h = \mu_m$. Therefore, eq. (D1) becomes:

$$\frac{P}{2\mu_{m}h} = \frac{6d_0^3}{b^4} + \frac{2d_0}{b^2} \,. \tag{D2}$$

Since Xu and Liechti (2011) assumed small membrane deflection, eq. (D2) should be compared with the Case I solution of free inflation in eq. (12) which gives

$$\frac{P}{2\mu_{m}h} = \frac{2d_{0}}{d_{0}^{2} + b^{2}}.$$
 (D3)

In Fig.16a, we compare eq. (D2) and (D3) and find that the two solutions agree when $d_0/b \ll 1$ (i.e., small deflection) but diverge when the membrane deflection increases (i.e., $d_0/b > 0.1$). This is expected since Xu and Liechti (2011) assumed linear elasticity and small deflection.

For contact with a flat rigid substrate, Xu and Liechti (2011) obtained the following relation between the internal pressure P and contact radius a under a fixed gap d_0 between the membrane edge and the substrate:

$$\frac{P}{2\mu_n h} = \frac{6d_0^3 C_1}{b^4 C_0^3} + \frac{2d_0}{b^2 C_0} \,. \tag{D4}$$

where

$$C_0 = 1 - (a/b)^2 + (a/b)^2 \ln(a/b)^2,$$
 (D5)

$$C_1 = 1 - 4(a/b)^2 + 3(a/b)^4 - (a/b)^4 \ln(a/b)^4.$$
 (D6)

Figure 16b and 16c show the comparison between eq. (D4) based on the solution of Xu and Liechti (2011) and our solution for two different gaps: $d_0/b = 0.01$ or 0.1. For $d_0/b = 0.01$ (see Fig.16b), eq. (D4) is in good agreement with our solution. When the gap is increased to $d_0/b = 0.1$ (see Fig.16c), our solution and eq. (D4) exhibit similar trends but a small deviation in the applied pressure P which originates from the diverging free inflation curves in Fig.16a under large deflection.

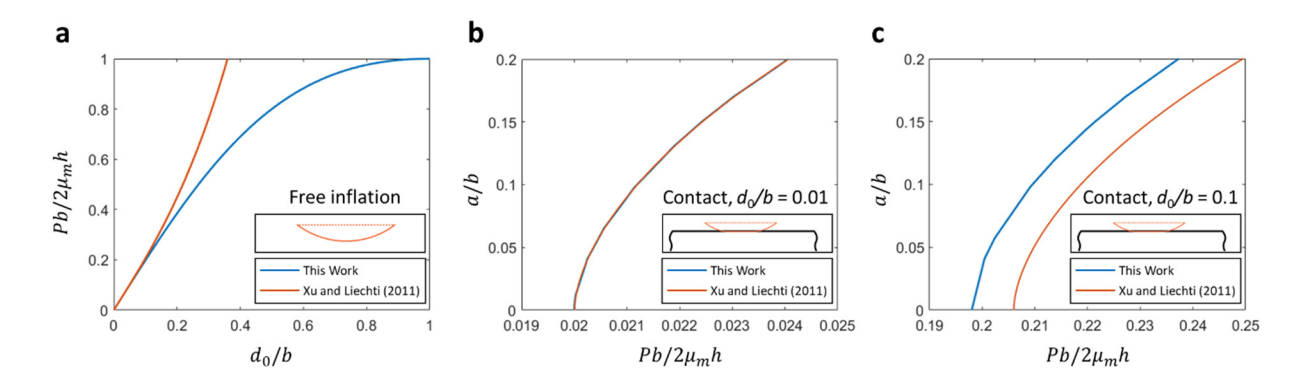


Figure 16 Comparison between the Case I solution for free inflation and contact with flat rigid substrate with the solution of Xu and Liechti (2011). The blue curves represent the solution from this work and the orange curves represent the solutions of Xu and Liechti (2011) with residual stress $\sigma_0 = \mu_m$. (a) Applied pressure versus membrane deflection under free inflation. (b-c) Contact radius versus applied pressure under a prescribed vertical gap of $d_0/b = 0.01$ and 0.1, respectively.

Appendix E: FEM simulations

Axisymmetric finite element models were established using the commercial software ABAQUS (version 2020, Simulia, Providence, RI, USA) to simulate the contact between the inflated membrane and various substrates. As illustrated in Fig. 17, the model included two parts: a thin circular membrane and a substrate underneath the membrane. The membrane, with a radius of $b/\lambda_0 = 1$ mm and a thickness of h = 1 µm in its undeformed state, was meshed with the 2-node linear axisymmetric shell elements (SAX1) with a uniform mesh size of 2 µm. The material model adopted for the membrane was the incompressible neo-Hookean solid with shear modulus $\mu_m = 2$ MPa. For the substrate, we considered 3 different geometries: a flat substrate (width = 2 mm and thickness = 1 mm; see Fig.17a), a spherically concave substrate (radius = 10 mm; see Fig.17b), and a spherically convex substrate (radius = 1 mm; see Fig.17c). All three substrates were meshed with axisymmetric continuum elements (CAX4H). The smallest elements, located at the top surface around the symmetry axis, were 1 μ m × 1 μ m in size, and the mesh size on the top surface of the substrate was no larger than 20 μm × 10 μm. To enable the consideration of substrate deformation (i.e., for the elastic substrates considered in Section 4), the substrates were modeled as an incompressible neo-Hookean solid which reduces to a linear elastic solid with Young's modulus E_s and Poisson's ratio $v_s = 1/2$ under infinitesimal deformation. For the rigid substrates considered in Section 3, E_s was set to be sufficient large (i.e., = 60 GPa) so that the substrate deformation was negligible.

Each simulation consisted of three steps. First, the membrane was pre-stretched equibiaxialy to reach the pre-stretch ratio λ_0 . Second, a uniform pressure was applied to inflate the membrane. Third, the substrate underneath the inflated membrane was moved upwards to make contact with the membrane in a quasi-static manner with the internal pressure P in the membrane kept constant. The static solver of ABAQUS/Standard was used for the first two steps. To improve convergence and accommodate potential instabilities, the third step was completed using the quasi-static solver of ABAQUS/Standard through the implicit dynamic analysis. Frictionless and adhesionless contact was applied to the interface between the membrane and the substrate.

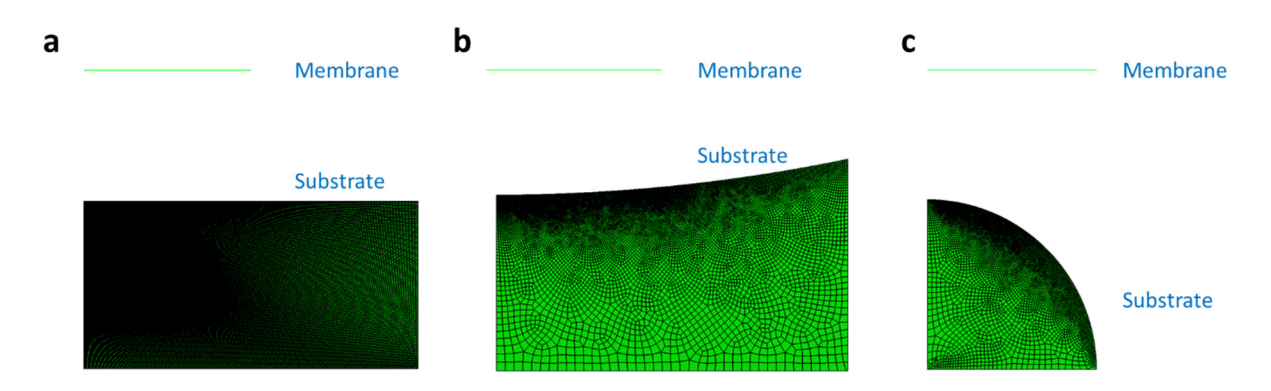


Figure 17 FEM models for membrane with (a) flat, (b)spherically concave and (c) spherically convex substrate.

References:

Carlson, A., Wang, S., Elvikis, P., Ferreira, P.M., Huang, Y., Rogers, J.A., 2012. Active, Programmable Elastomeric Surfaces with Tunable Adhesion for Deterministic Assembly by Transfer Printing. Adv. Funct. Mater. 22, 4476–4484.

Drotman, D., Jadhav, S., Karimi, M., Dezonia, P., Tolley, M.T., 2017. 3D printed soft actuators for a legged robot capable of navigating unstructured terrain, in: Proceedings - IEEE International Conference on Robotics and Automation. Institute of Electrical and Electronics Engineers Inc., pp. 5532–5538.

Feng, W.W., Yang, W.H., 1973. On the contact problem of an inflated spherical nonlinear membrane. J. Appl. Mech. Trans. ASME 40, 209–214.

Florez, J.M., Shih, B., Bai, Y., Paik, J.K., 2014. Soft pneumatic actuators for legged locomotion,

in: 2014 IEEE International Conference on Robotics and Biomimetics, IEEE ROBIO 2014. Institute of Electrical and Electronics Engineers Inc., pp. 27–34.

Foster, H.O., 1967a. Very large deformations of axially symmetrical membranes made of neo-hookean materials. Int. J. Eng. Sci. 5, 95–117.

Foster, H.O., 1967b. Inflation of a plane circular membrane. J. Manuf. Sci. Eng. Trans. ASME 89, 403–407.

Green, A.E., Adkins, J.E., 1960. Large elastic deformations and non-linear continuum mechanics. Clarendon Press.

Guo, J., Elgeneidy, K., Xiang, C., Lohse, N., Justham, L., Rossiter, J., 2018. Soft pneumatic grippers embedded with stretchable electroadhesion. Smart Mater. Struct. 27, 055006.

Hassager, O., Kristensen, S.B., Larsen, J.R., Neergaard, J., 1999. Inflation and instability of a polymeric membrane. J. Nonnewton. Fluid Mech. 88, 185–204.

Juhari, M.R., Ramasamy, R., Mamat, M.R., Yaacob, S., Mohd Nasir, N.F., Sugisaka, M., 2005. An Application of Finite Element Modelling to Pneumatic Artificial Muscle. Am. J. Appl. Sci. 2, 1504–1508.

Laprade, E.J., Long, R., Pham, J.T., Lawrence, J., Emrick, T., Crosby, A.J., Hui, C.Y., Shull, K.R., 2013. Large deformation and adhesive contact studies of axisymmetric membranes. Langmuir 29, 1407–1419.

Li, M., Luo, S., Nanayakkara, T., Seneviratne, L.D., Dasgupta, P., Althoefer, K., 2014. Multi-fingered haptic palpation using pneumatic feedback actuators. Sensors Actuators, A Phys. 218, 132–141.

Libai, A., Simmonds, J.G., 1998. The Nonlinear Theory of Elastic Shells, The Nonlinear Theory of Elastic Shells. Cambridge University Press.

Liu, M.X., Wang, C.G., Li, X.D., 2018. Rigid-flexible contact analysis of an inflated membrane balloon with various contact conditions. Int. J. Solids Struct. 144–145, 218–229.

Liu, T., Chiaramonte, M., Amini, A., Menguc, Y., Homsy, G.M., 2021. Indentation and bifurcation of inflated membranes. Proc. R. Soc. A Math. Phys. Eng. Sci. 477.

Long, R., Hui, C.Y., 2012. Axisymmetric membrane in adhesive contact with rigid substrates: Analytical solutions under large deformation. Int. J. Solids Struct. 49, 672–683.

Long, R., Shull, K.R., Hui, C.Y., 2010. Large deformation adhesive contact mechanics of circular membranes with a flat rigid substrate. J. Mech. Phys. Solids 58, 1225–1242.

Osborne, W.A., Sutherland, W., 1909. The elasticity of rubber balloons and hollow viscera. Proc. R. Soc. London. Ser. B, Contain. Pap. a Biol. Character 81, 485–499.

Patil, A., Dasgupta, A., 2013. Finite inflation of an initially stretched hyperelastic circular membrane. Eur. J. Mech. A/Solids 41, 28–36.

Patil, A., DasGupta, A., 2015. Constrained inflation of a stretched hyperelastic membrane inside an elastic cone. Meccanica 50, 1495–1508.

Patil, A., Dasgupta, A., Eriksson, A., 2015. Contact mechanics of a circular membrane inflated against a deformable substrate. Int. J. Solids Struct. 67–68, 250–262.

Patil, A., Nordmark, A., Eriksson, A., 2014. Free and constrained inflation of a pre-stretched cylindrical membrane. Proc. R. Soc. A Math. Phys. Eng. Sci. 470.

Rus, D., Tolley, M.T., 2015. Design, fabrication and control of soft robots. Nature 521.7553 (2015): 467-475.

Shepherd, R.F., Ilievski, F., Choi, W., Morin, S.A., Stokes, A.A., Mazzeo, A.D., Chen, X., Wang, M., Whitesides, G.M., 2011. Multigait soft robot. Proc. Natl. Acad. Sci. U. S. A. 108, 20400–20403.

Shintake, J., Cacucciolo, V., Floreano, D., Shea, H., 2018. Soft Robotic Grippers. Adv. Mater. 30.29 (2018): 1707035.

Sonar, H.A., Gerratt, A.P., Lacour, S.P., Paik, J., 2020. Closed-Loop Haptic Feedback Control Using a Self-Sensing Soft Pneumatic Actuator Skin. Soft Robot. 7, 22–29.

Song, K., Kim, S.H., Jin, S., Kim, S., Lee, S., Kim, J.S., Park, J.M., Cha, Y., 2019. Pneumatic actuator and flexible piezoelectric sensor for soft virtual reality glove system. Sci. Rep. 9, 1–8.

Song, S., Drotlef, D.-M., Majidi, C., Sitti, M., Rogers, J.A., 2017. Controllable load sharing for soft adhesive interfaces on three-dimensional surfaces. Natl. Acad Sci. 114.22 (2017): E4344-E4353.

Song, S., Drotlef, D.M., Paik, J., Majidi, C., Sitti, M., 2019. Mechanics of a pressure-controlled adhesive membrane for soft robotic gripping on curved surfaces. Extrem. Mech. Lett. 30, 100485.

Song, S., Sitti, M., 2014. Soft Grippers Using Micro-fibrillar Adhesives for Transfer Printing. Adv. Mater. 26, 4901–4906.

Srivastava, A., Hui, C.-Y., 2013. Large deformation contact mechanics of long rectangular membranes. I. Adhesionless contact. Proc. R. Soc. A Math. Phys. Eng. Sci. 469, 20130424.

Sun, Y., Guo, J., Miller-Jackson, T.M., Liang, X., Ang, M.H., Yeow, R.C.H., 2017. Design and fabrication of a shape-morphing soft pneumatic actuator: Soft robotic pad, in: IEEE International Conference on Intelligent Robots and Systems. Institute of Electrical and Electronics Engineers Inc., pp. 6214–6220.

Walker, J., Zidek, T., Harbel, C., Yoon, S., Strickland, F.S., Kumar, S., Shin, M., 2020. Soft robotics: A review of recent developments of pneumatic soft actuators. Actuators 9, 3.

Williams, J.G., 1997. Energy release rates for the peeling of flexible membranes and the analysis of blister tests. Int. J. Fract. 87, 265–288.

Xu, D., Liechti, K.M., 2010. Analytical and experimental study of a circular membrane in Hertzian contact with a rigid substrate. Int. J. Solids Struct. 47, 969–977.

Yang, W.H., Feng, W.W., 1970. On axisymmetrical deformations of nonlinear membranes. J. Appl. Mech. Trans. ASME 37, 1002–1011.

Yun, S.S., Kang, B.B., Cho, K.J., 2017. Exo-glove PM: An easily customizable modularized pneumatic assistive glove. IEEE Robot. Autom. Lett. 2, 1725–1732.

Zhong, G., Dou, W., Zhang, X., Yi, H., 2021. Bending analysis and contact force modeling of soft pneumatic actuators with pleated structures. Int. J. Mech. Sci. 193.